Contrib Mineral Petrol (2000) 140: 212–232

L. L. Perchuk · O. G. Safonov · T. V. Gerya
B. Fu · D. E. Harlov

Mobility of components in metasomatic transformation and partial melting of gneisses: an example from Sri Lanka

Received: 15 September 1999 / Accepted: 8 June 2000

Abstract Reaction textures, fluid inclusions, and metasomatic zoning coupled with thermodynamic calculations have allowed us to estimate the conditions under which a biotite–hornblende gneiss from the Kurunegala district, Sri Lanka [hornblende ($N_{Mg} = 38$–42) + biotite ($N_{Mg} = 42$–44) + plagioclase + quartz + K-feldspar + ilmenite + magnetite] was transformed into patches of charnockite along shear zones and foliation planes. Primary fluid inclusion data suggest that two immiscible fluids, an alkalic supercritical brine and almost pure CO_2, coexisted during the charnockitisation event and subsequent post-peak metamorphic evolution of the charnockite. These metasomatic fluids migrated through the amphibolite gneiss along shear zones and into the wallrock under peak metamorphic conditions of 700–750 °C, 5–6 kbar, and $a^{fl}_{H_2O} = 0.52$–0.59. This resulted in the formation of charnockite patches containing the assemblage orthopyroxene ($N_{Mg} = 45$–48) + K-feldspar ($Or_{70–80}$) + quartz + plagioclase (An_{28}) in addition to K-feldspar microveins along quartz and plagioclase grain boundaries. Remnants of the CO_2-rich fluid were trapped as separate fluid inclusions. The charnockite patches show the following metasomatic zonation patterns:

– a transition zone with the assemblage biotite ($N_{Mg} =$ 49–51) + hornblende ($N_{Mg} = 47$–50) + plagioclase + quartz + K-feldspar + ilmenite + magnetite;
– a KPQ (K-feldspar–plagioclase–quartz) zone with the assemblage K-feldspar + plagioclase + orthopyroxene ($N_{Mg} = 45$–48) + quartz + ilmenite + magnetite;
– a charnockite core with the assemblage K-feldspar + plagioclase + orthopyroxene ($N_{Mg} = 39$–41) + biotite ($N_{Mg} = 48$–52) + quartz + ilmenite + magnetite.

Systematic changes in the bulk chemistry and mineralogy across the four zones suggest that along with metasomatic transformation, this process may have been complicated by partial melting in the charnockite core. This melting would have been coeval with metasomatic processes on the periphery of the charnockite patch. There is also good evidence in the charnockitic core that a second mineral assemblage, consisting of orthopyroxene ($N_{Mg} =$ 36–42) + biotite ($N_{Mg} = 50$–51) + K-feldspar ($Or_{70–80}$) + quartz + plagioclase ($An_{28–26}$), could have crystallised from a partial melt during cooling from 720 to 660 °C at decreasing $a^{fl}_{H_2O}$ from 0.67 to 0.5. Post-magmatic evolution of charnockite at $T <$ 700 °C resulted in fluids being released during the crystallisation of the charnockitic core. These gave rise to the formation of late stage rim myrmekites along K-feldspar grain boundaries as well as late stage biotite, cummingtonite, and carbonates.

L. L. Perchuk (✉) · T. V. Gerya
Department of Geology, Moscow State University,
Vorobievy Gory, Moscow, 119899 Russia
e-mail: llp@geol.msu.ru

L. L. Perchuk · O. G. Safonov · T. V. Gerya
Institute of Experimental Mineralogy,
Russian Academy of Sciences,
Chernogolovka, Moscow district,
142432 Russia

B. Fu
Department of Petrology and Isotope Geology,
Vrije Universiteit, De Boelelaan 1085,
1081 HV Amsterdam, The Netherlands

D. E. Harlov
GeoForschungsZentrum,
Telgrafenberg, 14473 Potsdam, Germany
e-mail: dharlov@gfz-potsdam.de

Editorial responsibility: J. Touret

Abbreviations

X_{Mg}	Mg/(Mg + Fe)
X^{Bt}_{Eas}	0.5(Al–1)/[0.5(Al–1) + Fe + Mg]
X^{Opx}_{Al}	0.5Al/(0.5Al + Fe + Mg)
X^{Bt}_{F}	F/(F + Cl + OH)

X_{Or}^{Kfs}	K/(Ca + Na + K)
X_{An}^{Pl}	Ca/(Ca + Na + K)
μ_K^{+fl}	chemical potential of potassium ions in a fluid
μ_{Na}^{+fl}	chemical potential of sodium ions in a fluid
$a_{H_2O}^{fl}$	H_2O activity in a fluid
$f_{H_2O}^0$	fugacity of pure water
G	Gibbs free energy, cal/mol
H	enthalpy, cal
S	entropy, cal/mol/K
V	volume, cal/bar
R	1.987 cal/mol/K
$G^e(a)$	integral excess free energy, cal/mol
G_i^e	partial excess Gibbs' free energy of component i, cal/mol
W	the interaction parameters for a solid solution (s.s.)
Z	degree of ordering in Gibbs' K-feldspar

Introduction

Evidence that Na and K are 'perfectly mobile' during the transformation of amphibole–biotite gneiss into orthopyroxene-bearing granite (charnockitisation) includes K-feldspar reaction textures along quartz and plagioclase grain boundaries coupled with systematic zoning in both the feldspars and orthopyroxenes (cf. Korzhinskii 1959; Thompson 1959). The term 'perfectly mobile component' was introduced by Korzhinskii (1959) into the petrologic literature and is defined as a component whose chemical potential, $\mu_i = \mu_i^o + \mathrm{Rtln}a_i^{fl}$ is fixed at a given temperature and pressure by an external constraint on the system. Thus, from a thermodynamic point of view, the activity of a perfectly mobile component, like the pressure and temperature, is one of the constraints on the system. Korzhinskii (1962) proposed that charnockitisation was the result of an increase in the chemical potential of K^+ in a fluid, i.e. the perfect mobility of K^+, with respect to the reaction biotite + quartz + K_2O = orthopyroxene + K-feldspar + H_2O.

Perchuk and Gerya (1992, 1993) proposed that perfect mobility of the K_2O component in a fluid was most likely responsible for the transformation of amphibole–biotite gneiss into orthopyroxene-bearing granulite in a series of different granulite facies terranes. They suggested that an increase in the μ_{K2O} of a fluid would be reflected by systematic changes in the composition of the coexisting minerals via the following net-transfer reactions:

$$\underset{\text{Plagioclase}}{CaAl_2Si_2O_8 nNaAlSi_3O_8} + 1/2mK_2O \underset{\text{(fluid phase)}}{} = \underset{\text{Plagioclase}}{CaAl_2Si_2O_8(n-m)NaAlSi_3O_8} + \underset{\text{K-feldspar}}{mKAlSi_3O_8} + 1/2mNa_2O, \underset{\text{(fluid phase)}}{} \quad (1)$$

$$\underset{\text{Al-rich orthopyroxene}}{0.5(Fe,Mg)Al_2SiO_6} + 3SiO_2 + 1/2K_2O \underset{\text{(fluid phase)}}{} = \underset{\text{Al-free orthopyroxene}}{0.5(Fe,Mg)SiO_3} + \underset{\text{K-feldspar}}{KAlSi_3O_8}, \quad (2)$$

and

$$\underset{\text{Eastonite-Siderophillite}}{3K(Fe,Mg)_2Al_3Si_2O_{10}(OH)_2} + 21SiO_2 + 1/2K_2O \underset{\text{(fluid phase)}}{} = \underset{\text{Phlogopite-Annite}}{2K(Fe,Mg)_3AlSi_3O_{10}(OH)_2} + \underset{\text{K-feldspar}}{7KAlSi_3O_8} + H_2O, \quad (3)$$

Aspects of this model have consequently been supported by a number workers (e.g. Hansen et al. 1995; Newton 1995; Franz and Harlov 1998; Harlov et al. 1998; Newton et al. 1998; Safonov 1998; Harlov and Wirth 2000). The presence of alkali brine inclusions (Touret 1995a, b), K-feldspar microveins (Franz and Harlov 1998; Harlov and Wirth 2000), as well as K-feldspar microveins specifically associated with chlorine-rich minerals (Safonov 1998) in orthopyroxene-bearing granulites suggest that high alkali activity during metamorphism and charnockitisation is related to a low water activity, supercritical hypersaline alkalic fluid phase, i.e. a supercritical brine (cf. Aranovich et al. 1987; Shmulovich and Graham 1996; Aranovich and Newton 1997, 1998). Newton et al. (1998) has summarised the arguments for the role of these supercritical brines during high grade metamorphism and charnockitisation. In light of the above model we would then expect K-feldspar reaction textures and alkali brine fluid inclusions in the incipient (arrested) charnockites of southern India and Sri Lanka (cf. Safonov et al. 1999). Other workers, however, have suggested that charnockite formation, most notably in southern India, is essentially a metasomatic process involving the influx of a CO_2-rich (low H_2O activity) fluid through amphibolite facies gneisses along tectonically generated pathways (Friend 1981; Janardhan et al. 1982; Hansen et al. 1984, 1987; Newton 1986; Raith et al. 1989; Stähle et al. 1987; Santosh et al. 1990, 1991; Milisenda et al. 1991; Perchuk and Gerya 1992; Raith and Srikantappa 1993).

Rejecting the idea of high grade CO_2 metasomatism, at least on a local scale, Burton and O'Nions (1990) and Hiroi et al. (1990) have proposed that the arrested charnockites located in Kurunegala district, Sri Lanka, formed as a result of the partial melting of the original amphibolite facies gneisses. However, they neglect to provide direct evidence for partial melting such as melt inclusions, remnants of former melt veins or, more indirectly, indications of high water activity or high temperature that should be inherent in the local mineral assemblage. In this study we present new data on both reaction textures and fluid inclusions from a sample of arrested charnockite collected in the Kurunegala district, Sri Lanka, specifically from a charnockite patch in the Udadigana quarry. We demonstrate that while formation of these charnockite patches was most likely caused by the influx of a high grade fluid with both a CO_2 and a supercritical alkali brine component, partial melting could have occurred as a product of post-peak metamorphic processes shortly after the charnockitic patches had formed.

Rock description

In the Kurunegala district, Sri Lanka, biotite–hornblende granitic gneisses (560 Ma) of the Wanni Complex (Kröner et al. 1991; Mathavan et al. 1999) were partly converted into charnockite along narrow shear zones and foliation planes approximately 535 ± 36 Ma (Fig. 1a). The geology and petrography of the rocks from this area have been thoroughly described in a number of studies (e.g. Hiroi et al. 1990; Yoshida et al. 1990; Kröner et al. 1991; Yoshida and Santosh 1994; Mathavan et al. 1999). The transition from biotite–hornblende gneiss to charnockite can easily be seen in the outcrops by changes in the colour, texture and in the mineral modal composition of the rock. The charnockites form dark pods, veins and patches within the distinctly foliated light-grey granitic gneisses (Fig. 1a). The coarse-grained, recrystallised charnockite entirely obliterates the original gneissic foliation. Four major zones can be distinguished in each charnockitic 'patch' (Fig. 1b). These include:

- a distinctly foliated host gneiss consisting of hornblende + biotite + plagioclase + K-feldspar + quartz + ilmenite + magnetite;
- a transition zone with an inhomogeneous texture consisting of hornblende + biotite + plagioclase + K-feldspar + quartz + ilmenite + magnetite;
- a leucocratic zone consisting of K-feldspar + plagioclase + quartz (abbreviated as KPQ); and
- a charnockite core with an equigranular texture consisting of orthopyroxene + K-feldspar + quartz + plagioclase + biotite + magnetite + ilmenite + cummingtonite.

On weathered surfaces, the host gneiss shows a distinct foliation marked by hornblende and biotite. Locally, the rock contains large K-feldspar porphyroblasts and coarse-grained mesoperthitic alkali feldspar veins up to 1–2 cm thick. These veins are parallel to the foliation and contain inclusions of plagioclase, quartz, rare biotite and hornblende.

The thickness of the transition zone usually varies between 2 and 4 cm. The boundary between this zone and the host gneiss is not clearly defined (Fig. 1b). A faint foliation is still visible and disappears gradually towards the charnockite core along with a coarsening of both the quartz and feldspar grains. The biotite and hornblende grains loose their orientation and form elongated lenses, alternating with quartz–feldspar clusters.

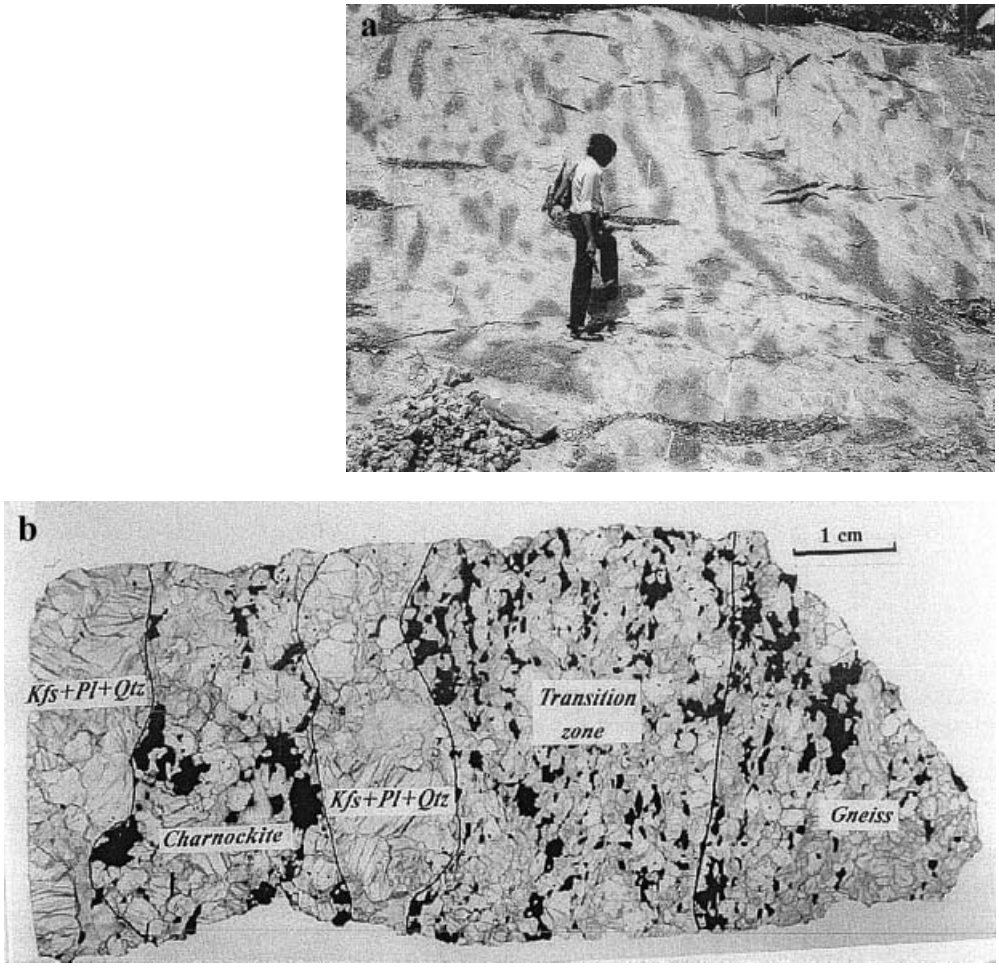

Fig. 1 **a** Arrested charnockite formation in the Kurunegala District, Sri Lanka (photo courtesy of Prof A. Kröner, Mainz). **b** An example of a typical charnockitic patch (sample SL-4/1) collected in the Udadigana Quarry (Kurunegala District, Sri Lanka). The four major zones include the host gneiss, the transition zone, the KPQ (K-feldspar + plagioclase + quartz) zone, and the charnockite core. The four zones are separated from each other by *solid lines*

The leucocratic quartz–feldspathic zone (KPQ) is marked by a significant increase in average grain size (Fig. 1b). Newly formed orthopyroxene, rare clinopyroxene and relict biotite do not exceed 3 vol%. Relics of biotite form inclusions in plagioclase. A few relatively large (up to 2 mm) orthopyroxene grains, partly replaced by secondary cummingtonite, appear at the contact with the charnockite core. These orthopyroxene grains were never observed in contact with biotite. K-feldspar grains (2–2.5 mm in size) in the KPQ zone have a strongly irregular shape and contain numerous plagioclase lamellae and inclusions of plagioclase and quartz. A spectacular feature of the KPQ zone is the presence of K-feldspar microveins along plagioclase and quartz grain boundaries (Fig. 2a). The thickness of these microveins varies from 50 to 300 μm. Thinner veins surround quartz and biotite inclusions in the plagioclase grains. Near the contact with the charnockite, these K-feldspar microveins partially envelop the orthopyroxene (Fig. 2b). They are completely absent in the surrounding amphibole–biotite gneiss.

The charnockite core has a homogeneous structure, reflecting the complete replacement of the gneiss (Fig. 1b). The charnockite is composed of K-feldspar, quartz, plagioclase, large euhedral grains (up to 4 mm) of orthopyroxene (~5 vol%), biotite and magnetite with ilmenite exsolution lamellae. Plagioclase in the charnockite forms grains of different shapes and sizes. The large grains contain numerous inclusions of K-feldspar, as well as quartz and biotite inclusions rimmed with K-feldspar. As a rule, these inclusions are only observed in the plagioclase cores, whereas the periphery of the plagioclase grains is inclusion free. The K-feldspar microveins are sporadically observed in some localised domains of the charnockite core as well. Apart from the microveins, individual K-feldspar grains occur as two morphological types. The first type includes large (up to 1–2 cm) partly broken phenocrysts with numerous plagioclase exsolution lamellae. The second type makes up the smaller K-feldspar grains in the matrix. The interior of these smaller grains often show a rash of tiny (3–7 μm) euhedral magnetite grains. Rim myrmekite is commonly found along K-feldspar grain boundaries growing into the K-feldspar (Fig. 2a; Fig. 3). A few mono-mineralic oligoclase microveins have also been observed.

Orthopyroxene and biotite are found in two types of associations in the charnockite core. In the first of these associations orthopyroxene (Opx1) and biotite are never in contact. This association is typically found in the KPQ zone. In the immediate vicinity of this association K-feldspar microveins along plagioclase and quartz grain boundaries are commonly found. In the second association, orthopyroxene (Opx2) is found as isolated grains as well as in contact with biotite. The K-feldspar microveins are rarely found in the immediate vicinity of this association.

Biotite in the charnockite occurs as three principle morphological types. These include small biotite inclusions (Bt1) rimmed by K-feldspar within large plagioclase or K-feldspar grains; relatively large crystals of biotite

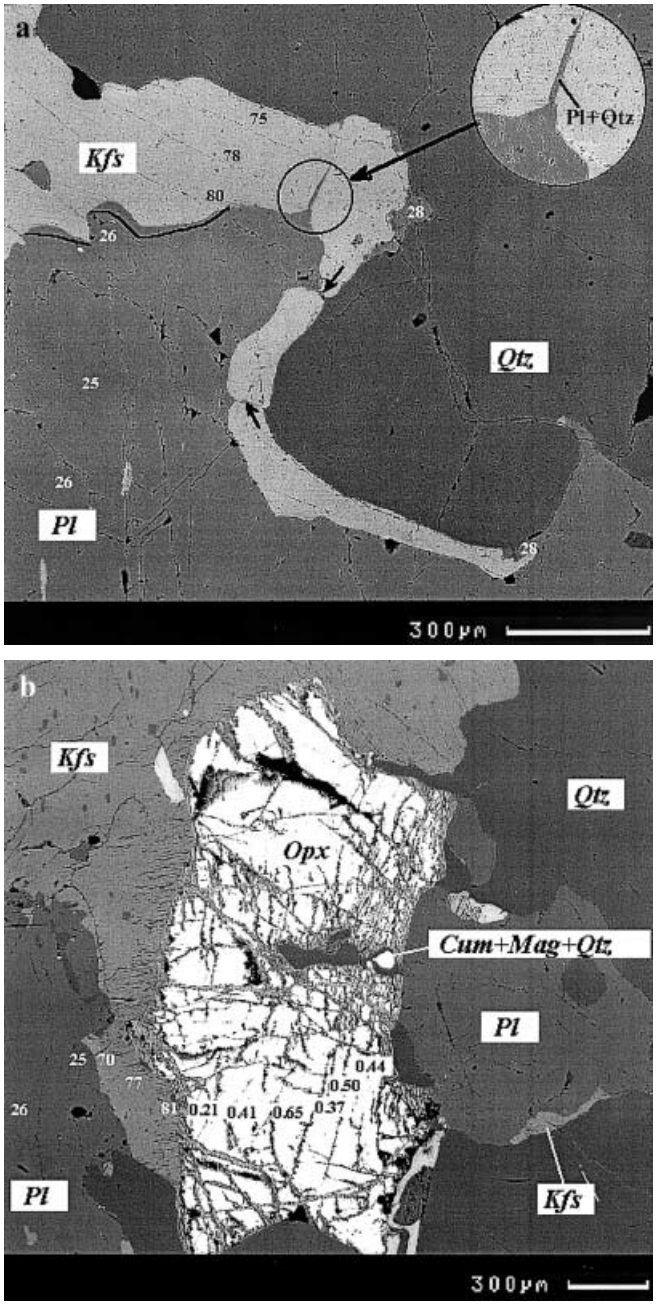

Fig. 2 BSE image showing the compositional and textural features of K-feldspar microveins in the KPQ zone of the charnockitic patch. **a** K-feldspar microvein between matrix plagioclase and quartz. The 20-μm-thick rim myrmekite (An23) intergrowth zone at the contact between the K-feldspar microvein and the matrix plagioclase is partly outlined by a *black line* as well as indicated by the black arrows. A close-up of the rim myrmekite at the grain boundary between two K-feldspar grains in the K-feldspar microvein is also shown. *Black numbers* in the K-feldspar microvein denote the orthoclase component. *White numbers* in the plagioclase and rim myrmekite denote the anorthite component. **b** K-feldspar reaction rim between orthopyroxene and plagioclase in the leucocratic KPQ zone. *White numbers* denote the anorthite component in the plagioclase and the orthoclase component in the K-feldspar. *Black numbers* denote the Al component in orthopyroxene

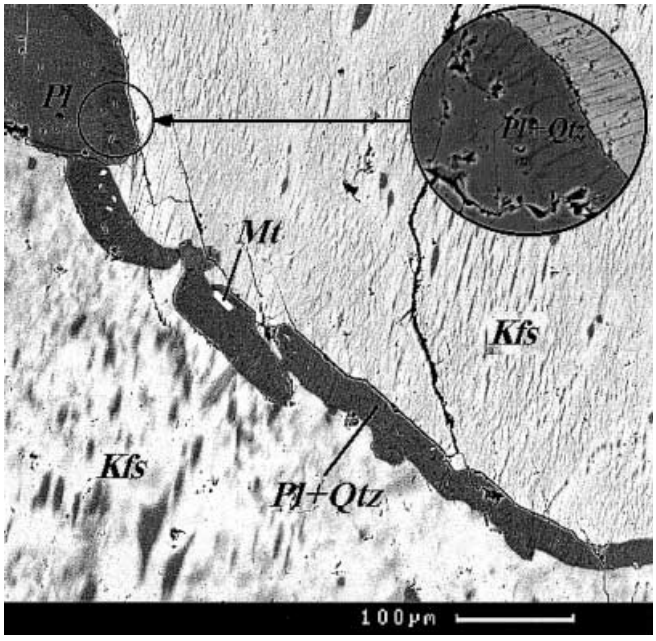

Fig. 3 BSE image of a rim myrmekite along a grain boundary between two mesoperthitic K-feldspar grains in the charnockite core. Here, the rim myrmekite takes the form of a migrating grain boundary into the K-feldspar

(Bt2) in contact with or replacing orthopyroxene as well as often being associated with biotite–quartz symplectites (Fig. 4); and lastly, flakes of biotite (Bt3) along cracks and grain boundaries within the charnockite core. Bt2 and Bt3

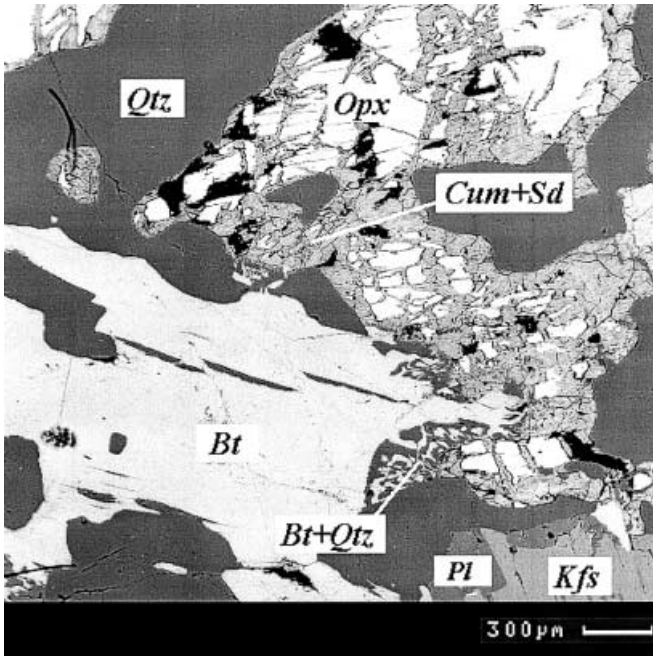

Fig. 4 BSE images of reaction textures indicating re-hydration in the charnockite core. These include biotite–quartz symplectites after orthopyroxene and K-feldspar; cummingtonite (*Cum*), quartz and siderite (*Sd*) after orthopyroxene; and secondary oligoclase developed after K-feldspar

are clearly post charnockitic replacing earlier charnockite minerals (most notably orthopyroxene).

Late alteration of minerals in the KPQ and charnockite zones includes partial replacement of the large, euhedral orthopyroxene crystals by cummingtonite, biotite and carbonates (ankerite, siderite and Ca-Mn carbonates) and very small grains of magnetite (Fig. 4). In addition, numerous tiny carbonate veins crosscut the plagioclase, quartz and K-feldspar grains. These veins frequently contain minute crystals of muscovite.

Analytical techniques

Minerals were analysed using both an electron microprobe JEOL Ltd. JXA-8800M at the Laboratorium Microanalyse of the Faculteit voor Aardwetenschappen, Vrije Universiteit Amsterdam (analyst W.J. Lustenhouwer) as well as a CamScan scanning electron microscope equipped with EDS Link AN10/85S at the Department of Petrology, Moscow State University (analysts E.V. Guseva and N.N. Korotaeva). The Link analyses were automatically normalised to 100%. Test analyses of the major elements for the same mineral grains using both instruments did not deviate from each other within ±1–2 wt%, i.e. microprobe error, for the major elements. A defocused beam (15 μm) was used to analyse the bulk composition of the antiperthitic K-feldspar. Biotite analyses were normalised to 7 (IV + VI) cations with $Fe^{3+} = \square^{A} + (Al^{IV}–1)–Al^{VI}–2Ti–Ca^{A}$. This assumes no octahedral vacancies. Pyroxene analyses were normalised to 2 (IV + VI) cations. Amphibole analyses were normalised to 13 (M1 + M2 + M3 + VI) cations with $Fe^{3+} = Al^{IV}–Al^{VI}–2Ti–Na^{A}–K + Na^{M4}$. Feldspar analyses were normalised to five cations.

The major element bulk chemistry for each zone was determined by using the following procedure. Twenty-two rock samples of ~2 × 2 × 1 cm in size were collected along two parallel traverses stretching from the host gneiss to the charnockite core (11 samples in each traverse). We were unable to separate a pure sample of either the charnockite core or the KPQ zone for bulk analysis. As a consequence, bulk analyses were made for samples that contained both a portion of the KPQ zone and the charnockite core in varying proportions. Each sample was reduced to a fine powder, which was subsequently placed into a graphite container. The powder was then melted in vacuum furnace at 1150 °C and quenched. Glasses were analysed using a defocused beam on the electron microprobe with each glass sample analysed three times. Table 1 shows the average composition of each sample.

The degree of ordering in the alkali feldspars were measured using unit-cell parameters. Unit-cell parameters were acquired from powder X-ray diffraction spectra (15 s/step; Co-anode and Fe-filter) in the Laboratory of X-ray Methods at the Institute of Experimental Mineralogy, Russian Academy of Sciences. Sample preparation consisted of separating out and then grinding up large K-feldspar grains to a fine powder (20–30 μm) and mixing them with an internal silicon standard.

Analyses using Raman spectroscopy were conducted using a multichannel laser Raman microspectrometer Dilor S.A. Microdil-28 in the Faculteit voor Aardwetenschappen, Vrije Universiteit, Amsterdam (analyst E.A.J. Burke).

Rock and mineral chemistry

Bulk rock chemistry

The zonation clearly visible in Fig. 1b corresponds to an overall depletion in mafic minerals within the KPQ–charnockite zone. This is verified by comparison

Table 1 Bulk rock chemistry

Sample	1	2	3	4	5	6	7	8	9	10	11
Zone	Gneiss	Gneiss	Trans. zone	Trans. zone	Charnockite	Charnockite	Charnockite	Charnockite	Trans. zone	Trans. zone	Gneiss
SiO_2	67.07	66.24	69.41	67.80	72.15	73.57	73.15	71.19	66.28	63.79	66.65
TiO_2	0.72	0.48	0.45	0.40	0.16	0.16	0.13	0.26	0.67	0.90	0.60
Al_2O_3	15.67	17.62	15.10	16.95	15.47	13.79	14.19	15.10	15.30	16.36	16.64
FeO	3.79	2.45	2.88	2.51	0.79	1.35	1.22	1.75	4.73	5.49	3.12
MnO	0.08	0.04	0.08	0.08	0.01	0.08	0.05	0.06	0.09	0.08	0.06
MgO	1.03	0.79	0.89	0.61	0.08	0.19	0.21	0.40	1.57	1.78	0.91
CaO	2.65	3.01	2.49	3.31	2.01	1.28	1.73	2.16	3.13	3.53	2.83
Na_2O	3.87	4.51	3.90	4.67	3.93	3.10	3.42	3.80	3.95	4.22	4.19
K_2O	4.53	4.50	4.39	3.21	4.98	5.94	5.03	4.71	4.06	3.60	4.52
Cl	0.1	0.06	0.05	0.08	0.03	0.06	0.13	0.07	0.05	0.07	0.08
S_2	0.46	0.27	0.34	0.37	0.38	0.43	0.53	0.41	0.16	0.10	0.37
Cr_2O_3	0.01	0.05	0.04	0.02	0.02	0.04	0.06	0.04	0.02	0.08	n.d.
Total	99.98	100.02	100.02	100.01	100.01	99.99	99.85	99.95	100.01	100.00	99.97
Normative (CIPW) composition											
Ab	41.5	48.1	40.5	50.4	37.4	28.5	31.8	37.3	45.0	51.2	44.8
Or	34.7	33.9	32.2	24.6	33.3	38.9	33.8	32.8	32.7	31.0	34.3
Qtz	23.9	17.9	27.3	25.0	29.2	32.6	34.4	29.9	22.2	17.8	20.8

of the bulk and normative rock analyses for each zone (Table 1). The charnockite core–KPQ zone is characterised by an appreciable increase in silica (Fig. 5a), a significant decrease in FeO, MgO and TiO_2 (Fig. 5b), and a decrease in CaO and Na_2O accompanied by K_2O enrichment (Fig. 5c). The silica content (68–70 wt%) of the gneiss is close to that of a granodiorite, but the chemical composition of the charnockite (71–73 wt%) corresponds to a typical granite. As a result, the whole rock composition of the charnockitic core corresponds to a granite minimum at P = 2–5 kbar and $a^{fl}_{H_2O} = 0.2$–0.4 (Ebadi and Johannes 1991). The charnockite is enriched in normative orthoclase with respect to the water-saturated granite minimum. This reflects a shift in the primary gneiss composition towards the water-undersaturated eutectic minimum (Fig. 6).

Mineral chemistry

The anorthite (An) content of matrix plagioclase from all zones varies from 23 to 28 (Table 2). Plagioclase in the charnockite is slightly more albitic ($An_{23–25}$) than plagioclase in either the gneiss or the transition zone ($An_{26–28}$). Large plagioclase grains in the charnockite core show some zonation. This ranges from $An_{27–28}$ in the cores, which contain biotite and K-feldspar inclusions, to $An_{25–26}$ in the inclusion-free rims. K-feldspar microveins in the KPQ zone contain plagioclase (An_{28}) inclusions (Fig. 2a). The most sodic plagioclase is observed in the rim myrmekites (Table 2) and ranges from An_{22} to An_{25} in the KPQ zone and An_{22} to An_{17} in the charnockite core.

K-feldspar grains from both the gneiss and the transition zone are relatively homogeneous in composition (Table 2). These K-feldspar grains contain thin lamellae of sodic plagioclase, whose composition is difficult to determine precisely because of their small (<3 μm) size. In contrast, K-feldspar grains from the KPQ zone and the charnockitic core show a wide range in composition ($Or_{70–90}$). In general, the K-feldspar grains from these two zones are more albite-rich than those from the gneissic or the transition zones (Table 2). K-feldspar grains in the charnockite contain numerous wide lamellae and spectacular euhedral inclusions of sodic plagioclase ($An_{19–21}$). In the KPQ zone, the orthoclase component in the K-feldspar microveins (Fig. 2a) systematically increases from the contact with quartz towards the contact with the matrix plagioclase. Measured unit-cell parameters for K-feldspar from the charnockite core are: a = 8.587 (±0.006) Å, b = 12.979 (±0.005) Å, c = 7.200 (±0.004) Å, $\beta = 116.05°$ (±0.005). The degree of ordering, Z ranges from 0.73 to 0.58 (mean 0.6) where $Z = -138.575 + 19.3153c_k$. Here, $c_{k=} c_{obs} + 0.038\ (1 - X^{Fsp}_K)$ and c_{obs} error is ±0.004 (cf. Hovis 1986).

There is a systematic change in the composition of the mafic minerals along the traverse from the host gneiss into the charnockite. The Mg content of biotite (N^{Bt}_{Mg}) in the gneiss and the transition zone is 40–44. The Al^{VI} content in its structural formula varies from 0.03 to 0.07 (Table 3). At the boundary between the transition and the KPQ zones, the N^{Bt}_{Mg} in biotite has increased to 49–51. This is almost 10 mol% higher than N^{Bt}_{Mg} for biotites in the gneiss and in the transition zones. In contrast, although N^{Bt}_{Mg} for small biotite inclusions rimmed by K-feldspar inside plagioclase from the KPQ zone is similar to that of biotite from the gneiss, the Ti content is lower (Table 3).

The three generations of biotite in the charnockite core differ significantly with respect to N^{Bt}_{Mg}.N^{Bt}_{Mg} for biotite inclusions in plagioclase enveloped by K-feldspar (Bt1) range from 40 to 47 (Table 3). Apparently, this biotite is a relic dating from the initial gneiss. The composition of Bt2 is more variable. Biotites in contact with

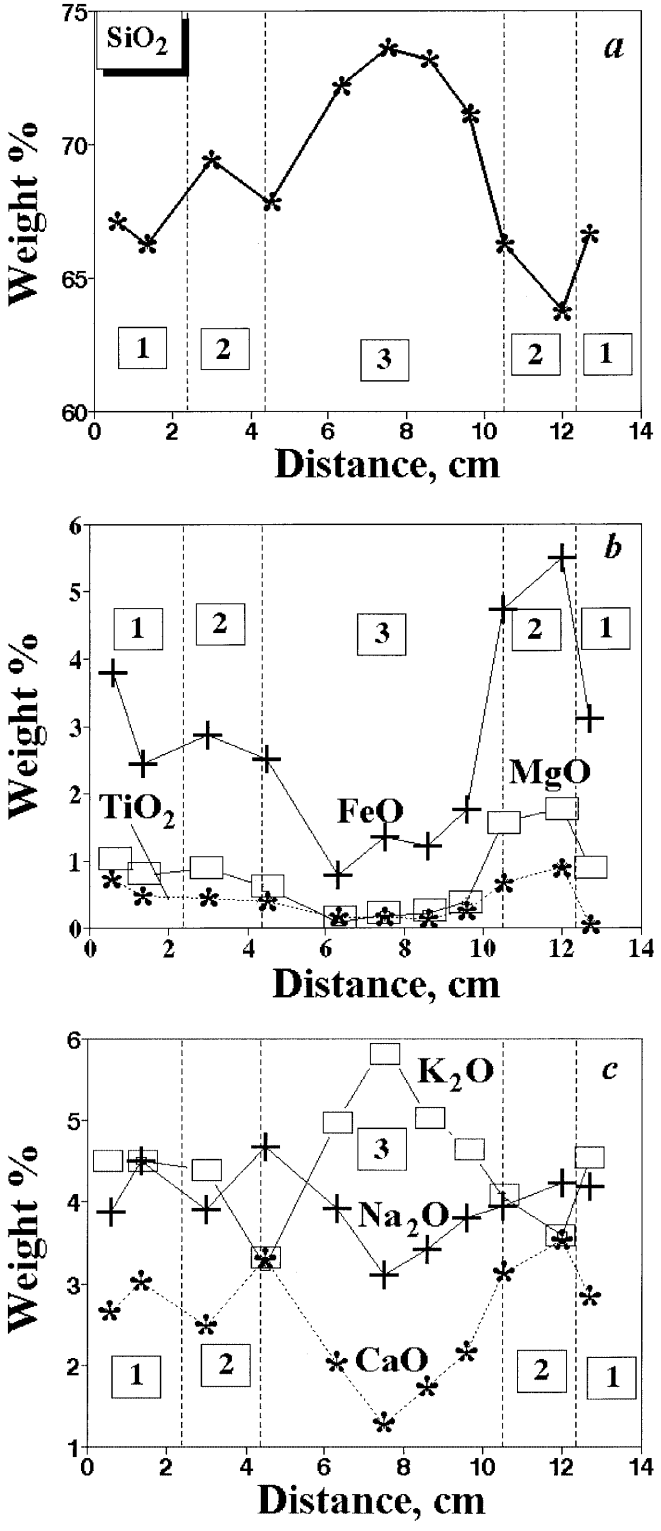

Fig. 5 Systematic change in bulk chemistry across the zonation of the charnockitic patch SL-4/1. These include **a** enrichment of the charnockitic-KPQ zone in SiO_2; **b** depletion of the charnockite–KPQ zone in FeO, MgO, TiO_2 with the accumulation of these components in the transition zone; and **c** decrease in CaO and Na_2O accompanied by an increase in K_2O in the charnockite–KPQ zone. *1* Hornblende–biotite gneiss; *2* transition zone; *3* charnockite/KPQ zone

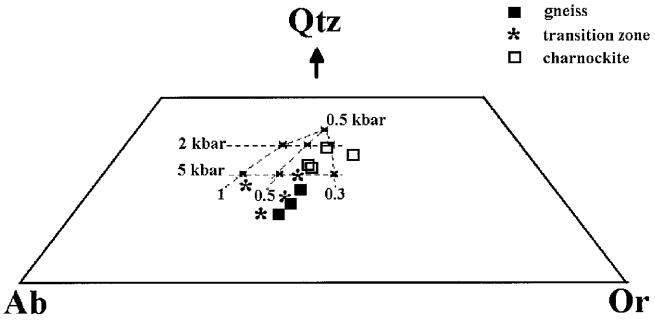

Fig. 6 Normative (Ab–Or–Qtz) composition across each of the three zones. The Ab–Or–Qtz normative composition for the charnockite (*white squares*) is displaced towards the granitic minimum at P = 2–5 kbar and a_{H_2O} = 0.5–0.2 (cf. Ebadi and Johannes 1991). *Crosses connected with dashed lines* mark the displacement of the granitic minimum with respect to P_{H_2O} at constant water activities of 1, 0.5 and 0.3 (*sub-vertical curves*) and by varying the water activity at constant pressures of 0.5, 2 and 5 kbar (*horizontal lines*)

orthopyroxene (N_{Mg}^{Opx} = 39–40) have values of N_{Mg}^{Bt} ranging from 46 to 51 (Table 3). Some of these biotite flakes are zoned. From core to rim N_{Mg}^{Bt} increases, whereas the Ti content decreases. N_{Mg}^{Bt} in the cores of such biotites typically average around 46–47 (Table 3) and presumably are relict biotites similar to Bt1. Locally, biotite with N_{Mg}^{Bt} = 58–59 are found in contact with Opx1 (N_{Mg}^{Opx} = 47). Bt3 (N_{Mg}^{Bt} = 49–52) is never found coexisting with orthopyroxene. Biotite from the quartz–biotite symplectites (N_{Mg}^{Bt} = 54–57) are poor in Ti. Biotites from all zones show a positive correlation of N_{Mg}^{Bt} with fluorine and are extremely poor in chlorine (Table 3).

Hornblende grains in both the gneiss and the transition zone have N_{Mg}^{Hbl} = 38–42 and contain ~0.1 Al atoms per VI site in the structural formula (Table 4). Similar to biotite, N_{Mg}^{Hbl} for the amphibole increases up to 46–47 at the boundary between the KPQ zone and the transition zone. Hornblende from the gneiss contains up to 0.7 wt% fluorine and, like the biotite, is also extremely poor in chlorine (Table 4). Hornblende has not been observed in the charnockite core. Secondary cummingtonite of N_{Mg}^{Cum} = 25 replaces orthopyroxene in both the charnockite and the KPQ zones (Table 4). It contains about 0.5 atoms of Ca and 0.85–0.89 atoms of Al per formula unit (normalised to 13 cations).

The two types of orthopyroxene (Opx1 and Opx2) from the KPQ zone and the charnockitic core have distinctly different compositions (Table 5). For large grains of Opx1 in both the KPQ zone and the charnockitic core, N_{Mg}^{Opx} = 45–48 and N_{Al}^{Opx} = 1.0–0.7 (Table 5). The Mg-number of Opx1 is similar to that of biotite and hornblende from the transition zone adjacent to the KPQ zone (compare analyses in Tables 3 and 4 with that of Table 5). Opx1 shows no regular zoning in the Mg and Fe content. However, at the contact with K-feldspar (Fig. 2b), the Al-content in Opx1 decreases systematically from the core (N_{Al}^{Opx} = 1.0–0.7) to the rim

Table 2 Feldspar analyses

Zone	Gneiss				Transition zone			Charnockite			
Analysis	GN6	GN7	GN4	GN5	TR21	TR32	TR29[a]	CH13	CH11	CH16[a]	CH17[a]
SiO_2	62.13	61.43	65.53	64.71	61.01	65.28	61.23	62.19	65.08	64.61	75.04
TiO_2	0.00	0.09	0.18	0.36	0.09	0.27	0.06	0.000	0.02	0.00	0.00
Al_2O_3	23.63	24.07	18.87	18.73	24.31	18.91	24.02	23.31	18.59	22.38	15.38
FeO	0.27	0.43	0.10	0.41	0.09	0.04	0.30	0.25	0.29	0.02	0.00
MnO	0.04	0.00	0.11	0.00	0.15	0.00	0.00	0.03	0.03	0.04	0.00
MgO	0.00	0.00	0.10	0.02	0.13	0.00	0.00	0.00	0.00	0.00	0.00
CaO	5.17	5.60	0.13	0.00	5.40	0.08	5.23	4.86	0.42	4.37	3.01
Na_2O	8.33	8.15	3.16	1.63	8.54	2.57	9.06	8.94	2.54	8.51	6.48
K_2O	0.41	0.20	11.79	14.05	0.28	12.85	0.10	0.43	12.99	0.07	0.09
Total	99.97	99.97	99.97	99.92	100.00	99.99	100.00	99.62	99.96	99.99	100.00
Formulae normalised to five cations											
Si	2.76	2.73	2.98	2.98	2.72	2.98	2.73	2.76	2.98	2.84	3.21
Ti	0.00	0.00	0.01	0.01	0.00	0.01	0.00	0.00	0.00	0.00	0.00
Al	1.24	1.26	1.01	1.01	1.27	1.02	1.26	1.22	1.00	1.16	0.78
Fe	0.01	0.02	0.00	0.02	0.00	0.00	0.01	0.01	0.01	0.00	0.00
Mn	0.00	0.00	0.00	0.00	0.01	0.00	0.00	0.00	0.00	0.00	0.00
Mg	0.00	0.00	0.01	0.00	0.01	0.00	0.00	0.00	0.00	0.00	0.00
Ca	0.25	0.27	0.01	0.00	0.26	0.00	0.25	0.23	0.02	0.21	0.14
Na	0.72	0.70	0.28	0.15	0.74	0.23	0.78	0.77	0.23	0.73	0.54
K	0.02	0.01	0.68	0.82	0.02	0.75	0.01	0.02	0.76	0.00	0.01
X_K	–	–	0.71	0.85	–	0.77	–	–	0.77	–	–
X_{ca}	0.26	0.28	–	–	0.26	–	0.24	0.23	–	0.22	0.20

[a] Plagioclase from the quartz–plagioclase microveins

($N_{Al}^{Opx} = 0.3$–0.2). The Ca-content in the Opx1 (Table 5) also decreases towards the rim, especially in the presence of secondary cummingtonite. Opx2 ($N_{Mg}^{Opx} = 36$–42; $N_{Al}^{Opx} = 0.5$–0.25) (Table 5) is always associated with biotite of $N_{Mg}^{Bt} = 47$–52. Rare clinopyroxene (Table 5) is observed in the KPQ zone only.

Table 3 Biotite analyses

Zone	Gneiss		Transition zone				Charnockite					
Analysis	GN24	GN23	TR1	TR2	TR3	TR4	CH19[a]	CH20[a]	CH5[b]	CH6[b]	CH13[c]	CH16[c]
SiO_2	35.64	35.81	36.66	36.71	36.89	36.74	36.68	36.53	36.83	36.91	37.09	36.92
TiO_2	5.18	5.15	5.24	5.25	5.11	4.92	4.71	4.81	5.05	5.18	4.21	4.09
Al_2O_3	12.76	12.75	12.98	13.09	13.08	13.06	12.95	12.90	13.01	13.11	13.40	13.17
FeO	23.81	22.28	22.55	22.50	22.57	22.98	24.36	24.30	21.73	21.75	20.03	19.98
MnO	0.22	0.23	0.22	0.24	0.20	0.21	0.24	0.21	0.21	0.20	0.23	0.23
MgO	9.03	10.02	10.16	9.91	10.03	9.87	9.33	9.25	10.62	10.68	11.82	11.99
CaO	0.01	0.00	0.01	0.00	0.02	0.00	0.00	0.00	0.01	0.02	0.00	0.00
Na_2O	0.11	0.10	0.13	0.12	0.10	0.12	0.06	0.03	0.13	0.11	0.12	0.08
K_2O	9.54	9.53	9.56	9.61	9.66	9.58	9.78	9.75	9.66	9.54	9.71	9.53
Cl	0.00	0.00	0.00	0.00	0.00	0.00	0.00	0.01	0.00	0.00	0.00	0.00
F	1.15	1.43	1.33	1.29	1.20	1.23	1.22	1.27	1.48	1.28	1.54	1.55
Total	97.44	97.31	98.83	98.71	98.86	98.70	99.34	99.06	98.71	98.77	98.16	97.54
Formulae normalised to seven cations												
Si	2.831	2.834	2.850	2.860	2.866	2.860	2.854	2.853	2.861	2.855	2.866	2.863
Ti	0.309	0.306	0.306	0.307	0.298	0.288	0.276	0.282	0.295	0.301	0.245	0.238
Al^{IV}	1.169	1.166	1.150	1.140	1.134	1.140	1.146	1.147	1.139	1.145	1.134	1.137
Al^{VId}	0.026	0.023	0.039	0.062	0.063	0.058	0.042	0.041	0.052	0.049	0.086	0.067
Fe^{3+d}	0.000	0.000	0.000	0.000	0.000	0.000	0.000	0.000	0.000	0.000	0.000	0.000
Fe^{2+}	1.581	1.474	1.465	1.465	1.465	1.495	1.585	1.586	1.411	1.406	1.294	1.296
Mn	0.015	0.015	0.014	0.016	0.013	0.014	0.016	0.014	0.014	0.013	0.015	0.015
Mg	1.069	1.181	1.176	1.150	1.160	1.145	1.082	1.076	1.229	1.231	1.360	1.385
Ca	0.001	0.000	0.000	0.000	0.002	0.000	0.000	0.000	0.000	0.002	0.000	0.000
Na	0.017	0.016	0.020	0.017	0.015	0.018	0.008	0.005	0.020	0.016	0.018	0.012
K	0.967	0.962	0.947	0.955	0.956	0.952	0.971	0.971	0.957	0.941	0.957	0.943
Cl	0.000	0.000	0.000	0.000	0.000	0.000	0.000	0.001	0.000	0.000	0.000	0.001
F	0.288	0.359	0.328	0.318	0.295	0.302	0.301	0.315	0.363	0.312	0.376	0.380
X_{Mg}	0.403	0.445	0.445	0.440	0.442	0.434	0.406	0.404	0.466	0.467	0.513	0.517

[a] Biotite inclusions inside plagioclase grains rimmed with K-feldspar
[b] Cores of primary biotite (see text)
[c] Biotite coexisting with Opx2 (see text)
[d] Calculated from normalised formula (see text)

Table 4 Amphibole analyses. *n.a.* Not analysed

Zone	Gneiss		Transition zone		Charnockite	
Analysis	GN26	GN27	TR13	TR33	A17[a]	A13[a]
SiO_2	41.93	42.30	42.11	43.51	48.46	48.36
TiO_2	2.20	2.06	2.19	2.14	0.22	0.24
Al_2O_3	9.86	9.84	10.31	10.21	5.23	5.47
FeO	21.34	21.35	22.19	19.77	32.93	33.77
MnO	0.58	0.56	0.55	0.42	2.26	2.16
MgO	8.33	8.32	8.25	9.66	6.80	6.41
CaO	10.69	10.94	10.85	11.04	3.58	3.33
Na_2O	1.91	1.88	2.07	1.90	0.21	0.00
K_2O	1.47	1.46	1.36	1.29	0.29	0.21
Cl	0.00	0.01	0.11	0.05	0.01	0.05
F	0.77	0.71	n.a.	n.a.	n.a.	n.a.
Total	99.08	99.42	100.00	100.00	99.99	99.99
Formulae normalised to 13 cations						
Si	6.343	6.382	6.277	6.397	6.677	6.647
Ti	0.250	0.233	0.246	0.237	0.023	0.024
Al^{IVb}	1.657	1.618	1.723	1.603	0.850	0.886
Al^{VIb}	0.101	0.132	0.089	0.165	0.000	0.000
Fe^{3+b}	0.748	0.657	0.822	0.705	0.810	0.801
Fe^{2+b}	1.950	2.036	1.943	1.725	2.983	3.079
Mn	0.075	0.072	0.070	0.053	0.263	0.251
Mg	1.876	1.871	1.832	2.116	1.395	1.311
Ca	1.732	1.767	1.732	1.739	0.529	0.490
Na^{VIb}	0.268	0.233	0.268	0.261	0.056	0.000
Na^{A}	0.292	0.316	0.331	0.280	0.000	0.000
K	0.284	0.280	0.259	0.241	0.051	0.036
Cl	0.000	0.002	0.028	0.013	0.002	0.011
F	0.370	0.340	n.a.	n.a.	n.a.	n.a.
X_{Mg}	0.410	0.410	0.393	0.460	0.256	0.241

[a] Secondary cummingtonite after orthopyroxene
[b] Calculated from normalised formula

Accessory minerals include magnetite, ilmenite, zircon, apatite, pyrite, pyrrhotite and allanite. These are observed in all four zones. Magnetite in the amphibole–biotite gneiss forms separate grains of ~1 mm in size, which contain ~2 wt% TiO_2 and about 0.7 wt% V_2O_3. Ilmenite ($N_{Hm}^{Ilm} = 8$–12) is also found in the amphibole-biotite gneiss both as single grains and as grains co-existing with magnetite. The KPQ zone contains both separate grains of magnetite and ilmenite as well as co-existing ilmenite and magnetite grains. Here the magnetite contains up to 2 wt% TiO_2 and about 0.4 wt% V_2O_3. In the charnockite core magnetite grains (up to 0.5 mm) contain numerous exsolution lamellae of ilmenite. Ilmenite also forms separate grains of 0.5 mm in size. Allanite is abundant in both the KPQ zone and the charnockite core.

Fluid inclusions

Most of the fluid inclusions observed in these zones are <10 μm. Many are secondary and have been considerably affected by explosion or implosion during retrograde evolution. Primary fluid inclusions are only found in K-feldspar and quartz from the KPQ zone and the charnockite core. In the charnockite core, quartz contains isolated primary-looking aqueous inclusions of predominantly 5–10 μm in size. The very irregular shape of these inclusions indicates conspicuous post-trapping changes (Roedder 1984). A typical volume ratio vapour/liquid in these inclusions is 0.1–0.2 (Fig. 7, plate 1). At room temperature these inclusions contain a thin liquid film and a small gas bubble squeezed around one or several isotropic and anisotropic solids (daughter crystals), which may occupy at least 80% of the cavity volume

Table 5 Pyroxene analyses. There are two generations of pyroxene in the charnockitic core: Opx1 includes A1 and A13; Opx2 includes D21, W4, W11 and K24

Zone	KPQ-zone			Charnockite					
Analysis	TR38	TR40	M6	A1	A13	D21	W4	W11	K24
SiO_2	49.78	49.69	51.58	49.67	49.71	48.69	49.42	49.63	49.08
TiO_2	0.12	0.04	0.55	0.09	0.00	0.08	0.08	0.06	0.03
Al_2O_3	0.63	0.78	1.01	0.83	0.72	0.49	0.45	0.36	0.37
FeO	31.37	31.80	12.62	31.37	30.94	35.04	34.50	34.44	35.17
MnO	1.57	1.76	0.50	1.64	1.62	1.90	1.75	1.77	1.82
MgO	15.44	15.14	11.58	14.87	15.18	12.60	12.84	12.90	12.32
CaO	0.99	0.73	21.55	1.52	1.40	0.94	0.95	0.81	0.95
Na_2O	0.08	0.02	0.56	0.00	0.29	0.24	0.00	0.00	0.00
K_2O	0.00	0.05	0.05	0.00	0.03	0.00	0.00	0.03	0.00
Total	99.99	99.98	100.00	99.98	99.89	99.97	100.00	100.00	99.74
Formulae normalised to two cations									
Si	0.974	0.974	0.987	0.973	0.976	0.974	0.984	0.988	0.983
Ti	0.002	0.001	0.008	0.001	0.000	0.001	0.001	0.001	0.000
Al	0.015	0.018	0.023	0.019	0.017	0.012	0.011	0.009	0.009
Fe	0.513	0.521	0.202	0.514	0.508	0.586	0.574	0.573	0.589
Mn	0.026	0.029	0.008	0.027	0.027	0.032	0.030	0.030	0.031
Mg	0.450	0.442	0.330	0.434	0.444	0.375	0.381	0.382	0.368
Ca	0.021	0.015	0.442	0.032	0.029	0.020	0.020	0.017	0.020
Na	0.003	0.001	0.021	0.000	0.011	0.009	0.000	0.000	0.000
K	0.000	0.001	0.001	0.000	0.001	0.000	0.000	0.001	0.000
X_{Mg}	0.467	0.459	0.620	0.458	0.466	0.391	0.399	0.400	0.384
X_{Al}	0.008	0.009	0.021	0.010	0.009	0.006	0.005	0.004	0.005

(Fig. 7, plate 2). This indicates that the cavity has literally collapsed around the enclosed solids and implies that during rock evolution the internal fluid pressure has been much lower than the rock pressure ('collapsed brines', Touret 1995a, b). The isotropic solids predominate. They show both cubic shapes (Fig. 7, plate 2) and an indistinct boundary at the quartz contact. Presumably these crystals are alkali chlorides, most likely halite (Fig. 7, plates 2, 3, and 5), as their refractive index is very similar to that of quartz. In some places it is very difficult to recognise the cubic contours of these solids. All attempts to determine whether or not these crystals were NaCl (at the polished surface) using the electron microprobe failed. Some isotropic crystals that have a more rounded irregular shape and lower refractive index are probably fluorite. Some anisotropic solids from the inclusions were identified as carbonates or bicarbonates (nahcolite).

Another type of primary fluid inclusion was observed in a large K-feldspar crystal that forms an isolated patch ~3 mm in diameter in the gneiss zone, near the transition zone (Fig. 7, plate 4). This perthitic feldspar is identical to those seen in the KPQ zone and is probably an outlier of the KPQ zone into the surrounding gneiss. Some of the K-feldspar crystals contain primary relatively large (up to 15 μm) CO_2-inclusions of which a few contain one or several solids. Two major types of solids were identified by Raman analysis. These include calcite crystals of variable size (Fig. 7, plates 6, 7, and 8) and rare small, <10 μm, K-feldspar crystals identical in its composition to the host K-feldspar (Fig. 7, plates 7 and 10). The occurrence of K-feldspar 'captured' crystals confirms the primary character of the fluid. The captured crystals are nuclei (seed crystals) that normally should have disappeared into the growing K-feldspar megacryst. These K-feldspar inclusions indicate that the fluid in these inclusions represent the original fluid in which the K-feldspar grew. The pure CO_2 composition of this fluid was verified by final melting temperature (T_m), which is close to the CO_2 triple point (i.e. −56.6 °C), as well as by Raman spectroscopy. Most of these inclusions homogenise to gas, but a few of them homogenise to liquid at +25 °C. The final melting of the CO_2 inclusions at the triple point corresponds to a molar volume of about 60 cm^3/mol. This indicates a fluid pressure of ~2 kbar for a reference temperature of 700 °C. However, it is evident that the initial CO_2 density was much higher. Most of the cavities are surrounded by spectacular near orthogonal microfractures developed along the cleavage planes in the host feldspar (Fig. 7, plate 11). These microfractures are probably channels for CO_2 leakage.

Brine and CO_2 inclusions were not observed in the gneiss and transition zones. These zones contain only trails of secondary inclusions with very irregular shapes and obvious signs of decrepitation. Some inclusions contain a low salinity aqueous fluid. The degree of fill is about 0.8–0.9, but most of the cavities are empty. Final melting temperatures are close to 0 °C, whereas the homogenisation to liquid occurs within the 120–190 °C temperature range. Late inclusions also occur in the charnockite core; however, they post-date the charnockitisation process.

Estimation of pressure and temperature

Numerous investigations have been made into the pressure–temperature (P–T) evolution of the arrested charnockites and accompanying host gneiss's from Sri Lanka (e.g. Hansen et al. 1987; Sandiford et al. 1988; Burton and O'Nions 1990; Schenk et al. 1991; Perchuk and Gerya 1992; Perchuk et al. 1994; Safonov et al. 1995). Estimations of pressure and temperature from these studies are relatively similar for a particular region despite the fact that different authors used different geothermobarometric databases. In this paper we utilise the GEOPATH internally consistent database (Gerya and Perchuk 1990a, b, 1992, 1994). For an independent test of the results we also applied other internally consistent databases such as Berman (1988), Holland and Powell (1990), and Berman and Aranovich (1996).

The lack of garnet in rocks from the Kurunegala quarry allows for, at best, a qualitative estimation of pressure. It forces us to use regional P–T estimations obtained by other workers for the Highland-Wanni crustal unit (cf. Hansen et al. 1987; Sandiford et al. 1988; Schenk et al. 1991; Safonov et al. 1995). From the P–T estimations contained in these references we have fitted the following equation as a function of temperature:

$$P\ (\text{kbar}) = 0.0178(\pm 3.391 \times 10^{-3})T(^\circ\text{C}) - 6.906(\pm 0.555) \qquad (4)$$

This estimation reflects the retrograde P–T path only and is practically identical (±0.05 kbar) to the 'united' decompression cooling P–T path fitted by Perchuk and Gerya (1992) for a series of different high-grade terrains:

$$P\ (\text{kbar}) = 0.0176(\pm 3.7681 \times 10^{-3})T(^\circ\text{C}) - 6.774(\pm 2.529) \qquad (5)$$

Because it represents a more general fit to high grade terranes, Eq. (5) will be used for pressure estimation.

Table 6 and Fig. 8 show temperatures calculated for the charnockite core using the orthopyroxene–biotite thermometer (cf. Fonarev and Konilov 1986; see also the Appendix). These temperatures, combined with Eq. (5), vary within the interval 690 ± 30 °C with a corresponding range in pressure of 4.3 to 6.2 kbar. The highest temperatures (710–740 °C) were calculated for biotite ($N_{Mg}^{Bt} = 58$–59, $TiO_2 = 4.5$–5.0 wt%) coexisting with Opx1 ($N_{Mg}^{Opx} = 47$; $N_{Al}^{Opx} = 0.9$). In contrast, for biotites co-existing with Opx2 in the charnockite core, estimated temperatures are <700 °C (Table 6).

Two feldspar thermometers were used in the estimation of temperatures in the charnockite. The first thermometer is based on the distribution of Na, K, and Ca between plagioclase and K-feldspar (Fuhrman and Lindsley 1988; Elkins and Grove 1990). The second feldspar thermometer takes into account the degree of ordering (Z) on the albite re-distribution between plagioclase and K-feldspar (Perchuk et al. 1990). Because


1

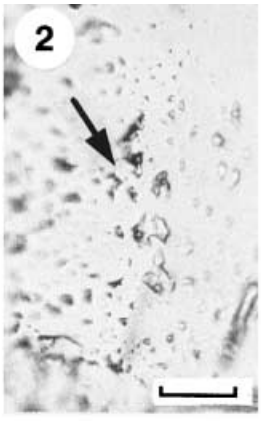
2

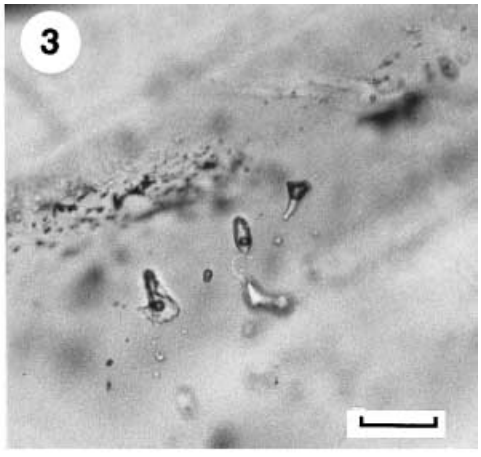
3

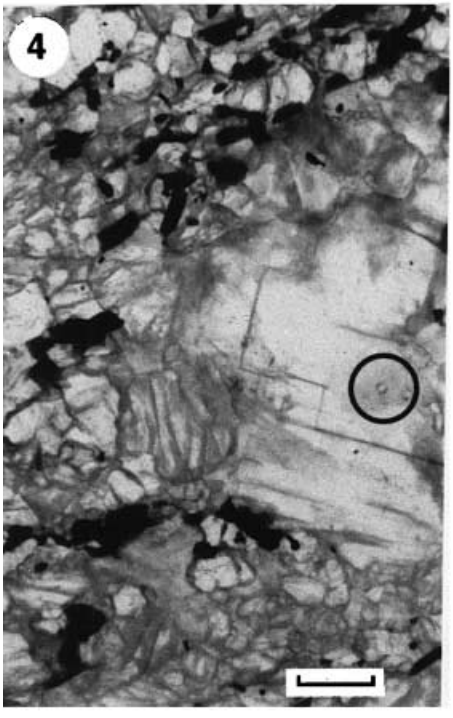
4

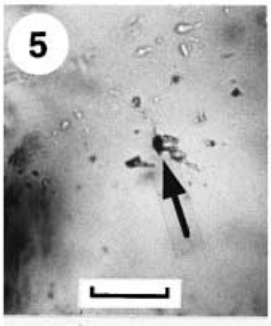
5

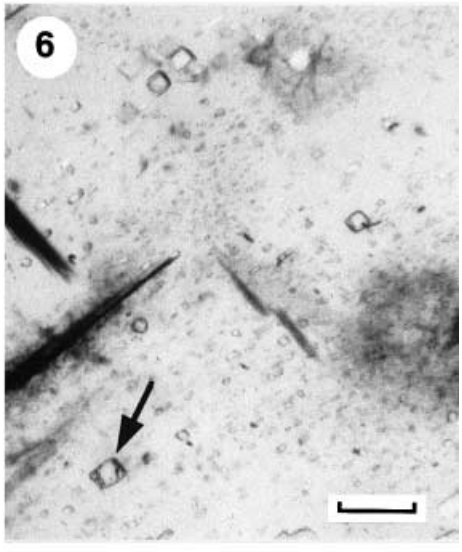
6

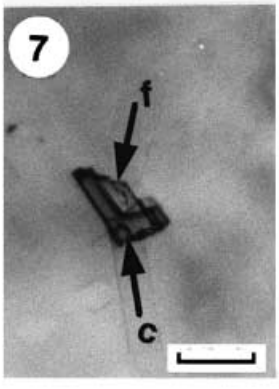
7
f
c

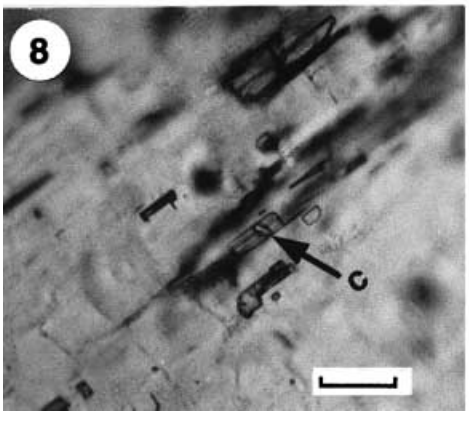
8
c


9

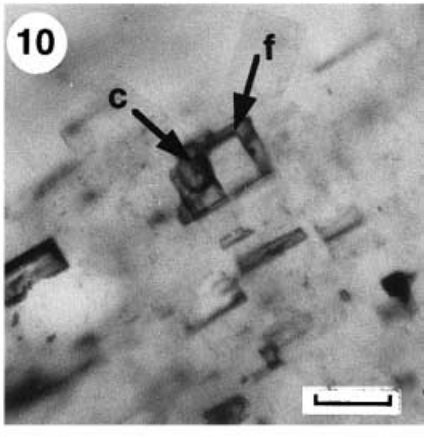
10
f
c

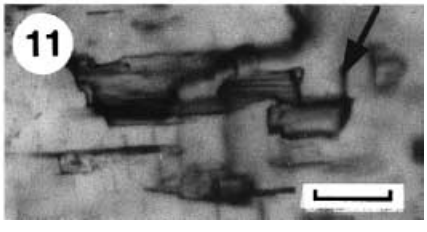
11

◄

Fig. 7 Fluid inclusions in the rocks studied. *Plate 1* Cluster of decrepitated irregular inclusions in quartz from the charnockite; *plate 2* group of collapsed inclusions containing very small vapour bubbles (<10% total volume) and a relatively large isotropic (halite) cube (*arrow*); *plate 3* group of isolated brine inclusions containing vapour bubbles (~15% of total volume), a liquid phase (NaCl-saturated liquid H_2O) and small halite crystals; *plate 4* K-feldspar phenocryst containing groups of CO_2-rich inclusions (*circle*); *plate 5* collapsed brine inclusions containing squeezed gas bubble (*black dot*) and halite cube (*arrow*); *plate 6* solid inclusions (mostly carbonates) and rectangular cavities containing large solids (K-feldspar, *arrow*) within the K-feldspar phenocryst; *plate 7* detail of fluid inclusion containing supercritical CO_2 (dark grey), *c* Mg-calcite and *f* feldspar crystals; *plate 8* group of inclusions containing supercritical CO_2 and a carbonate crystal (*arrow*); *plate 9* traces of empty inclusions (*dark*) regularly distributed within the host crystal (primary inclusions); *plate 10*: inclusion containing supercritical CO_2, *c* carbonate and *f* rectangular K-feldspar; *plate 11*: CO_2-rich inclusion surrounded by sub-orthogonal microfractures (*arrow*). For *plates 1*, *2*, *3*, *5*, *7*, *8*, *10*, and *11*, the length of the *bar* is 5 μm. For *plates 6* and *9* the length of the *bar* is 10 μm. For *plate 4* the length of the *bar* is 25 μm

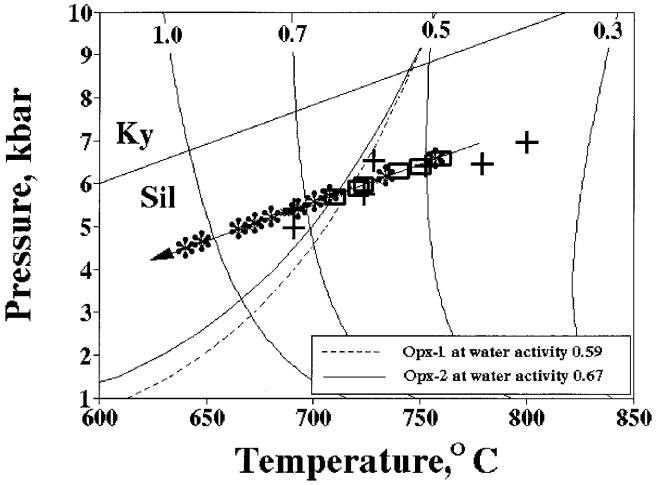

Fig. 8 P–T-$a^{fl}_{H_2O}$ diagram showing stability curves for Opx1 (*dashed line*) and Opx2 (*solid line*) with respect to the equilibrium biotite + quartz = orthopyroxene + K-feldspar + H_2O combined with solidus curves (*solid curves with negative slope*) for the granitic minimum at different water activities across the H_2O–CO_2 join (Ebadi and Johannes 1991). *Black crosses* indicate the P–T data of Schenk et al. (1991), Sandiford et al. (1988), Hansen et al. (1987), and Safonov et al. (1995). *Empty rectangles* denote P–T parameters calculated using the biotite–orthopyroxene thermometer combined with Eq. (5). *Asterisks* denote P–T parameters calculated from the two-feldspar thermometers combined with Eq. (5). *I* The peak pressure and temperature for charnockite formation at 700–740 °C. *II* Post peak metamorphic cooling

cooling generally leads to ordering in alkali feldspar, the measured value for Z corresponding to 0.6 probably corresponds to the stopping temperature for ordering in these feldspars (cf. Table 7). At higher temperatures, during peak metamorphic conditions, the value for Z was most likely lower, presumably close to zero. Assuming $Z = 0$ gives temperatures mostly above 700 °C. These show some agreement (±70 °C) with temperatures calculated using the biotite–orthopyroxene thermometer (cf. Table 7). If the measured value is used ($Z = 0.6$), the two-feldspar thermometer of Perchuk et al. (1990) gives considerably lower temperatures that vary between 530 and 560 °C. Application of this two-feldspar thermometer to myrmekites from the charnockitic core give temperatures that range from 440 to 550 °C (Table 8). This value is in good agreement with the lower limit established for myrmekite growth in general by Wirth and Voll (1987).

The composition of coexisting orthopyroxene, clinopyroxene and plagioclase grains from the KPQ zone were also used to estimate both temperature and pressure. Using thermodynamic data for pyroxenes and plagioclase from the database of Berman and Aranovich (1996), a temperature of ~700 °C and a pressure of ~6.3 kbar were estimated. These values are in good agreement with the results of calculations using the orthopyroxene–biotite thermometer and either feldspar thermometer in conjunction with the fitted pressure estimation represented by Eq. (5).

Pressure–temperature estimations contained in Tables 6, 7 and 8 and Fig. 8 suggest that peak meta-

Table 6 P–T-a_{H2O} parameters calculated from compositions of coexisting biotite and orthopyroxene from the charnockite core

Biotite					Orthopyroxene			K-feldspar		T, °C	P, kbar	a_{H_2O}
Analysis	N^{Bt}_{Mg}	$N^{Bt}_{Al(M1)}$	$N^{Bt}_{Ti(M1)}$	N^{Bt}_{F}	Analysis	N^{Opx}_{Mg}	N^{Opx}_{Al}	Analysis	N^{Kfs}_{K}			
A30	53.9	8.7	23.5	20.5	A28[a]	41.0	0.3	A25	87.3	675	5.1	0.470
A23	51.0	10.2	24.9	19.3	A22[a]	40.0	0.5	A21	73.3	698	5.5	0.633
A23	51.0	10.2	24.9	19.3	A29[a]	39.9	0.4	A26	80.2	697	5.5	0.590
A10	52.4	8.4	30.1	19.6	A18[a]	38.8	0.3	A16	75.6	628	4.3	0.417
D25	50.7	7.2	28.5	19.2	A18[a]	38.8	0.3	A16	75.6	660	4.8	0.507
D20	50.5	11.2	25.8	19.0	D21[a]	39.1	0.6	A16	75.6	671	5.0	0.541
D19	50.5	10.7	25.0	19.1	D21[a]	39.1	0.6	A16	75.6	668	5.0	0.527
A11	49.7	5.4	27.1	19.0	A12[a]	39.4	0.4	A20	86.7	727	6.0	0.672
D25	50.7	7.2	28.5	19.2	A15[a]	39.5	0.4	A16	75.6	683	5.2	0.573
A12	58.3	14.1	29.7	21.3	A13[b]	46.7	0.9	A16	80.9	716	5.8	0.535
A11	58.7	11.4	30.1	21.7	A13[b]	46.7	0.9	A16	80.9	711	5.7	0.519
A12	58.3	14.1	29.7	21.3	A14[b]	47.4	0.5	A16	80.9	737	6.2	0.589

[a] Opx1
[b] Opx2

Table 7 P–T parameters calculated from compositions of coexisting feldspars from the charnockite core

K-feldspar				Plagioclase				T °C[a]		T °C[b]	
Analysis	N_{Na}	N_{Ca}	N_K	Analysis	N_{Na}	N_{Ca}	N_K	F&L[c]	E&G[d]	Z = 0.6	Z = 0.0
W10	22.6	1.1	76.3	W5	73.7	23.7	2.6	669	640	535	665
D7	28.3	0.4	71.3	D10	73.4	23.9	2.6	694	713	563	759
5	24.4	0.2	75.4	L10	72.9	24.8	2.3	674	649	547	701
6	25.8	1.3	72.9	L10	72.4	24.8	2.7	688	710	556	730
11	25.8	1.0	73.1	L3	72.4	24.8	2.7	701	687	556	730
10	25.8	1.0	73.1	A6	71.9	25.8	2.3	693	681	558	735

[a] Average from T_{Or}, T_{An}, T_{Ab}
[b] Perchuk et al. (1990)
[c] Fuhrman and Lindsley (1988)
[d] Elkins and Grove (1990)

morphic conditions occurred at T > 700 °C and P > 5.5 kbar, resulting in the formation of Opx1 in both the metasomatic KPQ zone and in the charnockite core. These estimated peak metamorphic temperatures for the charnockite coincide with temperature estimations by Burton and O'Nions (1990) for the Kurunegala charnockites. Using magnetite–ilmenite, two-feldspar, and orthopyroxene–biotite thermometry, they concluded that charnockitisation took place at T = 738 ± 60 °C. Temperatures of 660–700 °C and pressures of <5.5 kbar correspond to a subsequent formation of Opx2 in close association with biotite in the charnockite core. Finally, the formation of rim myrmekite along K-feldspar grain boundaries and the replacement of both Opx1 and Opx2 by cummingtonite and carbonates mark the latest stage in the evolution of the charnockite core at temperatures of 440 to 550 °C and pressures of 1 to 3 kbar.

Discussion

Metasomatic reaction textures

The sample of charnockitised gneiss collected in the Udadigana quarry, Kurunegala district, Sri Lanka, as described in this study, contains a number of microtextures, which suggest metasomatic processes. They include K-feldspar microveins at the plagioclase–quartz and orthopyroxene–plagioclase grain boundaries (Fig. 2a, b), rim myrmekite in the K-feldspar along K-feldspar–plagioclase grain boundaries as well as along boundaries between the K-feldspar grains (Fig. 3), and late textures formed after the orthopyroxene and K-feldspar, i.e. biotite–quartz symplectites, cummingtonite–magnetite–quartz textures and carbonate veinlets (Fig. 4; Burton and O'Nions 1990; Perchuk et al. 1994).

Perchuk and Gerya (1992, 1993) proposed that similar K-feldspar microveins in charnockitised gneiss's from the Sulkava (southern Finland) and S.W. Baikal (Russia) complexes resulted from the following reaction:

$$(\text{Anorthite} * \text{nAlbite}) + \{\text{mK}^+\}^{\text{fl}} = (\text{Anorthite} * (\text{n} - \text{m})\text{Albite}) + \text{mOrthoclase} + \{\text{mNa}^+\}^{\text{fl}} \quad (6)$$

This reaction reflects an increase in the An content of the plagioclase at the contact with the K-feldspar microveins as a result of an increase in the potassium activity in a fluid. Similar relationships were later described by Hansen et al. (1995) in a charnockite from the Krishnagiri–Salem area (southern India).

In the case of the sample of charnockitised gneiss from the Udadigana quarry, the products of Eq. (6) are preserved locally. These include relict plagioclase grains of composition An_{28} as compared with plagioclase in the host gneiss, which has a compositional range of An_{24} to An_{26}. Relict plagioclase grains have been found along the K-feldspar microvein margin adjacent to the quartz grains (Fig. 2a) and in the plagioclase cores that contain K-feldspar inclusions. However, matrix plagioclase in contact with the K-feldspar microveins preserves a relatively constant composition, $An_{26–25}$, which is reflective of the host amphibolite facies gneiss (Fig. 2a). This would suggest that as the K-feldspar microveins grew, the orthoclase component increased while the composition of the original matrix plagioclase from the amphibolite gneiss remained relatively constant.

Two possibilities exist that could explain this constant composition. The first one would be an increase in

Table 8 Estimated P–T conditions of formation for selected rim myrmekites from the charnockite core

Analysis	N_{Na}^{Kfs}	Analysis	N_{Na}^{Pl}	T, °C[a]	P, kbar[b]
Z5	11.5	Z4	80.6	424	0.70
Z6	19.3	Z3	75.8	506	2.16
Z7	14.6	Z3	75.8	468	1.48
Z1	26.5	Z3	75.8	547	2.86
Z12	19.0	Z9	77.6	499	2.02
Z11	26.5	Z10	82.5	521	2.40
Z13	38.1	Z9	77.6	566	3.19
Z17	16.5	Z16	81.1	470	1.51
Z18	22.4	Z15	79.0	515	2.30
Z19	13.8	Z15	79.0	453	1.20
C11	17.9	C10	77.2	498	2.01
C11	17.9	C7	75.5	503	2.10
W16	11.9	W12	76.1	440	0.98
W16	11.9	W13	75.3	442	1.02

[a] Two feldspar thermometer (Perchuk et al. 1990) at Z = 0.6
[b] Equation (5), see text

the sodium activity in a fluid during the later stages of charnockitisation. In this case both feldspars would be enriched in albite. However, the K-feldspar microveins do not show any increase in the Ab content at the contact with the plagioclase. A second explanation is the net transfer reaction:

$$\underset{\text{Plagioclase}}{n\,CaAl_2Si_2O_8}\,\underset{}{(1-n)}\,\underset{}{NaAlSi_3O_8} + \underset{\text{Quartz}}{4n\,SiO_2} + \underset{\text{fluid}}{(m+2n)\,K^+}$$
$$= \underset{\text{K-feldspar}}{(1-n-m)\,NaAlSi_3O_8}\,\underset{}{(m+2n)\,KAlSi_3O_8} + \underset{\text{fluid}}{\{n\,Ca^{2+} + m\,Na^+\}} \quad (7)$$

Reaction (7) indicates that for the variable *m*, the Or content correlates positively with the potassium activity. The higher the activity of potassium in the fluid, the larger the amount of plagioclase is replaced by K-feldspar and the higher the orthoclase component in the newly formed K-feldspar. In contrast, the plagioclase composition remains constant because *m* is absent in the coefficient for the plagioclase molecule. The composition of the newly formed K-feldspar is then controlled by the following reaction:

$$\underset{\text{Albite}}{NaAlSi_3O_8} + \underset{\text{fluid}}{K^+} = \underset{\text{Orthoclase}}{KAlSi_3O_8} + \underset{\text{fluid}}{Na^+} \quad (8)$$

The formation of rim myrmekite intergrowths along K-feldspar microvein grain boundaries with plagioclase (Fig. 2a) suggests what is essentially a reverse of reaction (7) in conjunction with an alkali- and Ca-rich fluid.

Additional retrograde reaction textures include biotite–quartz symplectite, cummingtonite, magnetite and carbonate replacing orthopyroxene and K-feldspar. The formation of biotite–quartz symplectites after orthopyroxene and K-feldspar (Fig. 4) corresponds to rehydration of the orthopyroxene via the reaction 3 orthopyroxene + K-feldspar = biotite + 3 quartz, which proceeds to the right side with a decrease in temperature and/or an increase in the water activity. Replacement of orthopyroxene by cummingtonite (Fig. 4), again because of a decrease in temperature and/or increase in water activity, can be described by the reaction 7 orthopyroxene + quartz + H_2O = cummingtonite. This reaction can also occur in conjunction with the formation of secondary magnetite via two possible reactions, i.e. 48 ferrosilite + O_2 + H_2O = 6 cummingontie + 2 magnetite and 3 ferrosilite + 1/2 O_2 = magnetite + 3 quartz. Lastly, formation of siderite after orthopyroxene can be described by the reaction orthopyroxene + CO_2 = siderite + quartz. This reaction most likely explains the tiny carbonate veinlets observed in the plagioclase and K-feldspar. These carbonate veins are accompanied by the formation of secondary muscovite because of the reaction anorthite + K-feldspar + H_2O + CO_2 = muscovite + calcite + quartz. Each of these reaction textures point to an increase in the CO_2, H_2O and O_2 activities during retrograde metamorphism.

Water activities

Water activities ($a^{fl}_{H_2O}$) in the charnockite core during and after charnockitisation (Eq. (5) and Table 6) were estimated from co-existing biotite and orthopyroxene using the experimental data of Aranovich and Newton (1998; cf. Table A1 in the Appendix). The first group of water activities has a value of around $a^{fl}_{H_2O} = 0.59$ and corresponds to the formation of Opx1. The second group of water activities has a maximum value around $a^{fl}_{H_2O} = 0.67$ and corresponds to the formation of Opx2. This second group can be fitted to a linear equation:

$$a^{fl}_{H_2O} = 0.006246T(^\circ C) - 0.20536P(kbar) - 2.63312 \quad (9)$$

with $r^2 = 0.877$. The two groups of water activities indicate that although either generation of orthopyroxene (Opx1 and Opx2) in the charnockite core formed at the same temperature, they were stable at distinctly different water activities. In Fig. 8 are plotted the two $a^{fl}_{H_2O}$ isolines that delineate the stability fields of both generations of orthopyroxene. The calculated water activities for the formation and evolution of the Kurunegala charnockite are higher than previous estimates, i.e. $a^{fl}_{H_2O} < 0.35$ (cf. Hansen et al. 1987; Burton and O'Nions 1990; Perchuk et al. 1994; Safonov et al. 1999), which are based on the experimental data of Vielzeuf and Clemens (1992).

Aqueous brine inclusions are relatively more common in the charnockite core than CO_2-rich fluid inclusions. The abundance of isotropic solids in these brine inclusions imply high salinity in the fluid. Moreover, the isolated and clustered CO_2-rich inclusions that accompany the collapsed brine-rich inclusions point to an immiscibility between these two fluids, which indicates an initial high salinity for the fluid (Duan et al. 1995). Both fluids point to a relatively low water activity during charnockitisation.

The mole fraction of water in the brine can be roughly approximated from $X_{H_2O} = a_{H_2O}/\gamma_{H_2O}$ where a_{H_2O} is taken from Table 6 and γ_{H_2O} is take from Aranovich and Newton (1997). For the temperature interval 740–660 °C this yields a value for $X_{H_2O} = 0.78$–0.64, which is in good agreement with an increase in the immiscibility gap in the H_2O–NaCl–CO_2 system for decreasing pressures and temperatures (cf. Duan et al. 1995).

Alkali activities

Opx1 ($N_{Mg} = 45$–48 and $N_{Al} = 0.65$–1.0) appears in the KPQ zone only at the contact with the charnockite core. Replacement of hornblende or biotite by orthopyroxene was not observed in the transition zone. Moreover, in the KPQ zone, N_{Mg} for both the biotite and the hornblende are close to that of Opx1. This suggests that Opx1 most likely originated from the biotite + hornblende assemblage. Such a transformation cannot be explained by a change in pressure–temperature conditions but

rather by relatively high alkali activities in a fluid, because, at low alkali activities, fluid–rock interaction would yield an excess of Al_2SiO_5.

Taking into account the actual compositions of the co-existing biotites, hornblendes, and orthopyroxenes, the metasomatic transformation into charnockite of patches of biotite–amphibole gneiss in the Udadigana quarry can be described by the following reactions:

$$\underset{\text{Biotite}}{K(Fe,Mg)_{2.88}Al_{1.24}Si_{2.88}O_{10}(OH)_2} + \underset{\text{Quartz}}{3.563\ SiO_2} + \underset{\text{Fluid}}{0.188K^+} = \underset{\text{Orthopyroxene}}{1.453(Mg,Fe)_{1.982}Al_{0.036}Si_{1.982}O_6} + \underset{\text{K-feldspar}}{1.188KAlSi_3O_8} + 0.906H_2O + 0.188H^+ \quad (10)$$

and

$$\underset{\text{Biotite}}{K(Fe,Mg)_{2.88}Al_{1.24}Si_{2.88}O_{10}(OH)_2} + \underset{\text{Hornblende}}{0.057(K_{0.3}Na_{0.7})Ca_2(Mg,Fe)_{4.6}Al_{1.8}Si_{6.6}O_{22}(OH)_2} + \underset{\text{Quartz}}{3.743SiO_2}$$
$$+ \underset{\text{Fluid}}{0.011K^+ + 0.217Na^+} = \underset{\text{Orthopyroxene}}{1.586(Mg,Fe)_{1.982}Al_{0.036}Si_{1.982}O_6} + \underset{\text{K-feldspar}}{1.286(K_{0.8}Na_{0.2})AlSi_3O_8} + \underset{\text{Fluid}}{1.057H_2O + 0.114Ca^{2+}} \quad (11)$$

These reactions confirm the similar N_{Mg} content (~50 mole%) in the biotites, hornblendes and orthopyroxenes as well as differences in their Al content in the zones adjacent to the KPQ zone. Reactions (10) and (11) also demonstrate that the formation of the K-feldspar (Or_{80}) + Opx1 ($N_{Al} = 0.9$) assemblage in the KPQ zone is caused by an increase in the alkali activity of the fluid that reacted with the biotite, hornblende and quartz. Figure 2b suggests that a decrease in the Al-content from the core to the rim in both Opx1 and Opx2 can be explained via reaction (2). Reaction (2) operates simultaneously with reactions (1), (6), and (7), which are responsible for the formation of the K-feldspar microveins. In the charnockite core this event is followed by a slight increase in the alkali (and calcium) activities in the fluid at T<600 °C and P = 3 kbar. This most likely resulted in the formation of post-peak metamorphic rim myrmekite along the K-feldspar grain boundaries (Fig. 3).

Equilibria (1), (2) and (3) (see also equilibria R1, R8 and R9 in Table A1, Appendix) allow for the calculation of alkali activities during charnockitisation. These calculations, however, greatly depend on which anionic species might be present in the fluid. Both the mineral composition and the fluid inclusion data strongly suggest that the fluid contained Cl, F, and CO_2-bearing species only. Unfortunately, the specific ionic forms of these species as well as that of potassium and sodium are unknown. As a first approximation estimation of alkali activities were carried out in terms of K^+ and Na^+.

Figure 9a, b show the results of these calculations in the form of a subsolidus diagram with the co-ordinates $\log_{10}(a_{K^+}/a_{H^+})^{fl}$ and $\log_{10}(a_{Na^+}/a_{H^+})^{fl}$. The method used in these calculations is given in the Appendix and used both whole rock and mineral compositions (Tables 1, 2, 3, 4, and 5) as well as thermodynamic data from Table A1 (see Appendix). The systematic change in the aluminium contents of the newly formed orthopyroxene (Fig. 2b), as well as the composition of the coexisting feldspars were also taken into account. The diagrams in Fig. 9 allow for the projection of the stability fields for various mineral assemblages as a function of the variability in the potassium and sodium activities at constant temperature, pressure, and water activity (Fig. 8).

Figure 9a is calculated for mean values of T = 720 °C, $a^{fl}_{H_2O} = 0.55$, and $N^{rock}_{Mg} = 0.4$. At these values, Opx1 (N^{Opx}_{Mg} = 45–48 and N^{Opx}_{Al} = 0.65–1.0) is not stable with biotite and the divariant field for orthopyroxene + biotite + K-feldspar + plagioclase + quartz is highly suppressed. This is seen in Fig. 9a where the arrow reflects a decrease in the Opx1 Al-content along with an increase in N^{Kfs}_{K}. This was observed in both the orthopyroxene and the K-feldspar microveins along their contact (Fig. 2b). Such a compositional evolution corresponds to an increase in both $\log_{10}(a_{K^+}/a_{H^+})^{fl}$ and $\log_{10}(a_{Na^+}/a_{H^+})^{fl}$. In contrast, Opx2 ($N^{Opx}_{Mg}$ = 39–41 and N^{Opx}_{Al} = 0.6–0.5) can coexist with biotite at 680 °C and $a_{H_2O} = 0.55$. Figure 9b illustrates their phase relationship using the co-ordinates $\log_{10}(a_{K^+}/a_{H^+})^{fl}$ and $\log_{10}(a_{Na^+}/a_{H^+})^{fl}$ for $N^{rock}_{Mg} = 0.4$. In comparison with the diagram in Fig. 9a, the orthopyroxene + biotite + K-feldspar + quartz + plagioclase stability field in Fig. 9b is greatly extended.

Partial melting

According to Ebadi and Johannes (1991), the bulk chemistry data from Table 1 and Fig. 6 indicate that the composition of the charnockitic core is close to that of a water-undersaturated granite minimum. This means that for the estimated peak temperature and pressure of about 740 °C and 6 kbar (Table 6), melting could occur at a water activity of ~0.6. Calculated water activities, using this same bulk chemistry, suggest a maximum value for $a^{fl}_{H_2O}$ of 0.59 (Table 6) during the formation of Opx1. As a consequence, Opx1 could not have coexisted with a melt. This suggests that it formed metasomatically and was preserved during post-peak metamorphic evolution of the charnockite core. In

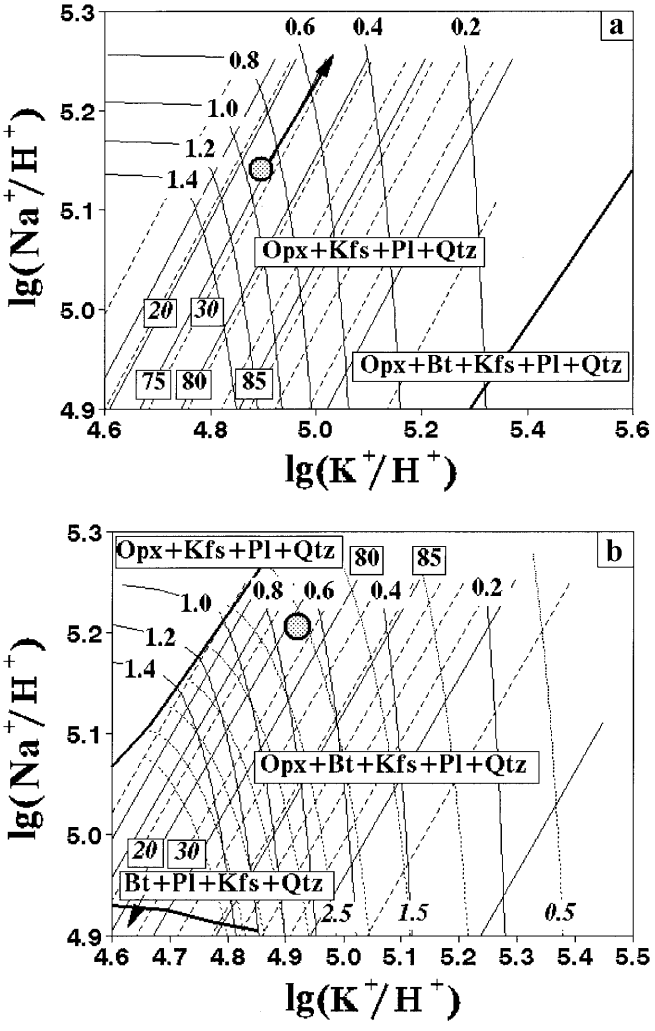

Fig. 9 The $\log_{10}(a_{K^+}/a_{H^+})^{fl} - \log_{10}(a_{Na^+}/a_{H^+})^{fl}$ diagrams for the equilibrium orthopyroxene ± biotite + K-feldspar + plagioclase + quartz assemblage in equilibrium with an H_2O fluid containing K^+, Na^+, and H^+. **a** Orthopyroxene + K-feldspar + plagioclase + quartz + fluid equilibria at 720 °C for $a_{H_2O} = 0.55$ and $N^{rock}_{Mg} = 0.4$. **b** Orthopyroxene + biotite + K-feldspar + plagioclase + quartz + fluid equilibria at 680 °C, $a_{H_2O} = 0.55$, and $N^{rock}_{Mg} = 0.4$. The *black arrow* in **a** shows an increase in the chemical potential of the alkalis during charnockitisation. This increase in the chemical potential is recorded in the zoning of Al in Opx1 (see text). Isopleths include N^{Kfs}_{Or} (*solid lines with boxed labels*); N^{Pl}_{An} (*dashed straight lines with italic boxed labels*); N^{Bt}_{Eas} (*steep dashed lines with italic labels*) extending from the biotite + quartz field into the orthopyroxene + K-feldspar + biotite + quartz + plagioclase field, and N^{Opx}_{Al} (the *steeply curved solid lines with normal labels*) extending from the orthopyroxene + K-feldspar + plagioclase field into the orthopyroxene + K-feldspar + biotite + quartz + plagioclase field. *Black bold lines* in the diagrams indicate the borders of the divariant field orthopyroxene + biotite + K-feldspar + plagioclase + quartz. *Shaded areas* show the compositions of co-existing minerals in the charnockite and corresponding $\log(a_{K^+}/a_{H^+})^{fl}$ and $\log(a_{Na^+}/a_{H^+})^{fl}$ values

contrast, the temperature and pressure intervals of 700–750 °C and 5–6 kbar at $a^{fl}_{H_2O} = 0.67$ correspond to a stability field for Opx2 that could have included a melt (Fig. 8). The amount of Opx2 in the charnockite is ~5 vol%, which is significantly less than the amount of biotite and hornblende in the protolith, i.e. the hornblende–biotite gneiss. The stability field for the cotectic assemblage melt + Opx2 + biotite within the charnockitic core could be even broader because of the presence of additional components. For example, the fluorine content in biotites from the Kurunegala quarry indicate that the amount of fluorine in the melt at 700 °C was ~0.3 wt% (Icenhower and London 1997). According to the experimental data of Manning (1981), the introduction of 0.3 wt% F into a H_2O-saturated granitic system leads to a decrease of about 20 °C in the melting temperature.

Conclusions

Reaction textures, fluid inclusions, as well as the rock and mineral chemistry imply that formation of the charnockite core was essentially a metasomatic process caused by the influx of an external complex fluid, with both a CO_2 and supercritical brine component, which migrated through these gneiss's along shear zones at temperatures and pressures of 700–750 °C and 5–6 kbar. With changing fluid compositions this process may have been complicated by partial melting. An external source for the fluid is supported by the isotopic data of Jackson et al. (1988) and Hoernes et al. (1991). Recently, Kehelpannala and Ratnayake (1999) have described the formation of K-feldspar-biotite–magnetite rocks after the same biotite–hornblende orthogneisses from the Ambagaspitiya area, which are structurally very similar to the Kurunegala arrested charnockite formation. They propose that these rocks also formed because of metasomatism with a K^+-rich fluid.

The formation of charnockite patches includes two metasomatic mechanisms: influx of the fluid along shear zones and diffusive migration of a fluid into the wall-rocks. Because of fluid–rock interaction, the following metasomatic zonation appeared along these shear zones and foliation planes in the amphibole–biotite gneiss [hornblende (N_{Mg} = 38–42) + biotite (N_{Mg} = 42–44) + plagioclase + quartz + K-feldspar + ilmenite + magnetite]:

- a transition zone with the assemblage biotite (N_{Mg} = 49–51) + hornblende (N_{Mg} = 47–50) + plagioclase + quartz + K-feldspar + ilmenite + magnetite;
- a KPQ zone with the assemblage K-feldspar + plagioclase + orthopyroxene (N_{Mg} = 45–48) + quartz + ilmenite + magnetite; and
- a charnockite core with the assemblage K-feldspar + plagioclase + orthopyroxene (N_{Mg} = 39–41) + biotite (N_{Mg} = 48–52) + quartz + ilmenite + magnetite.

Peak metamorphic conditions occurred at T = 700–750 °C, P = 6.5 kbar, and $a^{fl}_{H_2O} = 0.52$–0.59. This resulted in the assemblage orthopyroxene (N_{Mg} = 45–48)

+ K-feldspar ($Or_{70–80}$) + quartz + plagioclase (An_{28}), which formed metasomatically via reactions (1), (2), (3), (7) and (8) starting in the KPQ zone at the 'charnockitisation front'. Primary fluid inclusion data, coupled with thermodynamic data, suggest that two immiscible fluids, i.e. an alkalic supercritical brine and almost pure CO_2, coexisted at peak metamorphic conditions during the charnockitisation event and subsequent post-peak metamorphic evolution of the charnockite. The supercritical brine component was most likely responsible for the formation of the K-feldspar microveins in the KPQ zone and locally in the charnockite core, whereas remnants of the CO_2-rich fluid component were trapped as separate inclusions.

Systematic changes in the bulk chemistry and mineralogy across the four zones suggest that metasomatic transformation could have led to partial melting in the charnockite core. This melting would have been coeval with metasomatic processes on the periphery of the charnockite patch. The assemblage orthopyroxene ($N_{Mg} = 36–42$) + biotite ($N_{Mg} = 50–51$) + K-feldspar ($Or_{70–80}$) + quartz + plagioclase ($An_{28–26}$) in the charnockitic core would have then crystallised from a melt during cooling from 720 to 660 °C at decreasing $a^{fl}_{H_2O}$ from 0.67 to 0.5. The post-magmatic evolution of the charnockite at $T < 700$ °C is related to a fluid released during the crystallisation of the charnockitic core. This fluid gives rise to the formation of late rim myrmekite along K-feldspar grain boundaries, late biotite, cummingtonite, and carbonates.

The model described here is similar to one previously outlined by Perchuk and Gerya (1992) and Perchuk et al. (1994) for the formation of regional charnockite bodies and charnockite–enderbite complexes. In both cases charnockite formation is characterised by a similar geochemistry, similar reaction textures, high alkalis mobility and similar P–T-a_{H_2O} parameters. The implication, then, is that the localised charnockite patches in the Kurunegala quarry could serve as a micro-model for the formation of large-scale Precambrian charnockite complexes.

Acknowledgements Facilities for electron microprobe and Raman analyses were provided by the Departments of Petrology at Moscow State University and the Vrije Universiteit Amsterdam in cooperation with the Netherlands Organization for Scientific Research (NWO). We thank Ms E.V. Guseva and Ms N.N. Korotaeva (Moscow State University) and Mr W.J. Lustenhouwer (VUA) for microprobe analyses, Drs E.A.J. Burke (VUA) for the Raman analyses. We also thank Dr A.V. Chichagov (Institute of Experimental Mineralogy RAS) for X-ray measurements of K-feldspars in the charnockite and Prof. A. Kröner (Mainz) for providing the photo of the Kurunegala quarry. Special thanks are due to R.C. Newton for his support (Newton 1995) of an idea (Perchuk and Gerya 1993) on the role of mobility of alkalis in charnockitisation. Several versions of this manuscript have been greatly improved by critics and comments from M. Raith (Bonn), L. Ya. Aranovitch (Moscow) and several anonymous reviewers. The author's research is supported by the INTAS Foundation (grant 94-3138), and Russian Fund for Basic Research (Grants 96-15-98470 and 99-05-65602 to L.L.P., and 99-05-65451 to O.G.S.).

Appendix

A1 Calculations of temperature and water activity during charnockitisation

Temperature, pressure and water activity during formation of the charnockite were calculated simultaneously by means of combining reactions r7 and r5 from (A1) with Eq. (5) (see text). Tables A1 and A2 present the thermodynamic data for the reactions used. The equilibrium constant for reaction r5 is given by:

$$K_{(r5)} = (a^{fl}_{H_2O})^{1/3} a^{Opx}_{En} a^{Kfs}_{San^{1/3}}) / a^{Bt}_{Phl^{1/3}} = \exp(-\Delta G^{o}_{(r5)}/RT) \qquad (A1)$$

where

$$\Delta G^{o}_{(r5)} = \Delta H^{o}_{(r5)} - T\Delta S^{o}_{(r5)} + P_s \Delta V^{o}_{(r5)} + 1/3RT\ln f^{o}_{H_2O}$$

Table A1 compiles the data on $\Delta H^{o}_{(r5)}$, $\Delta S^{o}_{(r5)}$, and $\Delta V^{o}_{(r5)}$. The equilibrium constant for reaction r7 (Table A1) is:

$$K_{(r7)} = (a^{Opx}_{Fs} a^{Bt}_{Phl^{1/3}}) / (a^{Opx}_{En} a^{Bt}_{Ann^{1/3}}) = \exp(-\Delta G^{o}_{(r7)}/RT) \qquad (A2)$$

where

$$\Delta G^{o}_{(r7)} = \Delta H^{o}_{(r7)} - T\Delta S^{o}_{(r7)} + P_s \Delta V^{o}_{(r7)}$$

Here, $\Delta H^{o}_{(r7)}$, $\Delta S^{o}_{(r7)}$ and $\Delta V^{o}_{(r7)}$ are given in Table A1.

Orthopyroxene

The following one-site activity model was applied to calculate mixing properties for orthopyroxene:

$$RT\ln a_{En} = RT\ln(X_{En}) + G^{e}_{En} \text{ and } RT\ln a_{Fs} = RT\ln(X_{Fs}) + G^{e}_{Fs}$$

The partial molar excess Gibbs' free energies of enstatite and ferrosilite in the orthopyroxene solid solution, $G^{e}_{En} = RT\ln\gamma_{En}$ and $G^{e}_{Fs} = RT\ln\gamma_{Fs}$, were calculated using the following formulation for the Gibbs' excess energy (Gerya and Perchuk 1992):

$$\begin{aligned} G^{e}(Opx) = {} & X_{En}X_{Fs}[W^{G}_{MgFe} + (X_{en} - X_{Fs})W^{G}_{FeMg}] \\ & + X_{En}X_{Al}W^{G}_{MgAl} + X_{Fs}X_{Al}W^{G}_{FeAl} \end{aligned} \qquad (A3)$$

where

$$W^{G}_{ij} = W^{H}_{ij} - TW^{S}_{ij} + PW^{V}_{ij};$$

$$X_{En} = Mg/(Mg + Fe + Al/2);$$

$$X_{Fs} = Fe/(Mg + Fe + Al/2);$$

$$X_{Al} = 0.5Al/(Mg + Fe + Al/2);$$

and

$$X_{Al} + X_{Fs} + X_{En} = 1 \ .$$

The interaction parameters, W^{H}_{ij}, W^{S}_{ij} and W^{V}_{ij}, are given in Tables A1 and A2.

Biotite

Fe–Mg mixing in biotite was assumed to approximate ideality (cf. Gerya and Perchuk 1992) or:

$$a^{ideal}_{Phl} = (X_{Phl})^3 (X_{OH})^2 \qquad (A4\text{-}1)$$

$$a^{ideal}_{Ann} = (X_{Ann})^3 (X_{OH})^2 \qquad (A4\text{-}2)$$

Table A1 Thermodynamic data for reactions used for calculations of temperature, water activity, a_{K+}/a_{H+} and a_{Na+}/a_{H+} ratios in a fluid equilibrated with the charnockite. *OK* 'orthocorundum' or a fictive orthopyroxene end member (Al_2O_3)

Reaction index/reference[a]	Reaction	ΔH^0 (cal/mol)	ΔS^0 (e.u.)	ΔV^0 (cal/bar)
r1 (1)	$Ab + K^+ = Kfs + Na^+$	−5024	−3.651	0.0160
r2 (2, 3)	$Sil + 2K^+ + H_2O + 5Qtz = 2Kfs + H^+$	−14689	−66.9	0.776
r3 (4)	OK + Qtz = Sil	−5049	0.358	−0.0279
r4 (7)	1/3Eas[b] + Qtz = 1/3Kfs + OK + $1/3H_2O$	7971	12.874	−0.1745
r5 (5)	1/3Phl + Qtz = 1/3Kfs + En + $1/3H_2O$	8488	12.87	−0.11839
r6 (4)	1/3Phl + OK = 1/3Eas + En	140	−1.282	−0.0322
r7 (6)	1/3Ann + En = 1/3Phl + Fs	−3472	2.866	−0.0054
r8 (8)	$OK + 2K^{++}6Qtz = 2Kfs + 2H^+$	−19712.1	−66.2771	−1.8284
r9 (9)	OH-Phl + F-Ann = OH-Ann + F-Phl	0	−4.399	0

[a] *1* Calculated after data of Perchuk et al. (1990); *2* Shock and Helgeson (1988), Shock et al. (1989); *3* Holland and Powell (1990); *4* Gerya and Perchuk (1992); *5* Aranovich and Newton (1998); *6* calculated using experimental data of Fonarev and Konilov (1986); *7* combination of reactions r3 with r2; *8* combination of reactions r3 with r2; *9* Aranovich (1991)
[b] Fictive 'eastonite', $KAl_7O_{10}(OH)_2$

Table A2 Thermodynamic data for reactions used for calculations of temperature, water activity, a_{K+}/a_{H+} and a_{Na+}/a_{H+} ratios in a fluid equilibrated with the charnockite

Interaction parameter	W^H (cal/mol)	W^S (cal/mol/K)	W^V (cal/bar)	Reference
Orthopyroxene s.s.				
W_{MgFe}	−1652	−0.835	0	Gerya and Perchuk (1992)
W_{FeMg}	303	−0.269	0	
W_{MgAl}	0	0	0	Gerya and Perchuk (1992)
W_{FeAl}	−2527	0	−0.0309	Gerya and Perchuk (1992)
Biotite s.s.				
W_{MgAl}	−4405	0	0	Gerya and Perchuk (1992)
W_{FeAl}	−24577	0	0	Gerya and Perchuk (1992)

where

$X_{Phl} = Mg/(Mg + Fe + (Al\text{-}1)/2);$

$X_{Ann} = Fe/(Mg + Fe + (Al\text{-}1)/2);$

and

$X_{OH} = (1 - F - Cl)/2$.

Here, cation values are calculated using a biotite formula (Mg + Fe + Ti + Al + Si) normalised to seven cations.

Non-ideal energy contributions include Mg–Fe–Al mixing on the M site and reciprocal solid solution effects. This results in additional terms being added to (A4-1) and (A4-2) or:

$$RT\ln a_{Phl} = RT\ln a_{Phl}^{ideal} + (G_{Mg}^e)^M + X_{Ann}X_F\Delta G_{A5}$$

$$RT\ln a_{Ann} = RT\ln a_{Ann}^{ideal} + (G_{Fe}^e)^M - X_{Phl}X_F\Delta G_{A5}$$

Here, ΔG_{A5} [= −4.399T (cal)] is the free energy for the following internal exchange reaction:

$$\text{OH-phlogopite} + \text{F-annite} = \text{OH-annite} + \text{F-phlogopite} \quad (A5)$$

(cf. r10 in Table A1; Aranovich 1991). The partial mixing functions $(G_{Mg}^e)^M$ and $(G_{Fe}^e)^M$ are calculated from integral mixing function $G^e(Bt)$ or:

$$G^e(Bt) = W_{MgAl}^G X_{Phl}X_{Eas} + W_{FeAl}^G X_{Ann}X_{Eas} \quad (A6)$$

This assumes regular mixing between Mg and Al and between Fe and Al (Gerya and Perchuk 1992). Here,

$W^G = W^H - TW^S + PW^V;$

$X_{Phl} = Mg/(Mg + Fe + (Al - 1)/2);$

$X_{Ann} = Fe/(Mg + Fe + (Al - 1)/2);$

$X_{Eas} = (Al - 1)/2/(Mg + Fe + (Al - 1)/2);$

and

$X_{Ann} + X_{Phl} + X_{Eas} = 1$

for a formula normalised to seven cations. The values of interaction parameters W^H, W^S, and W^V are given in Table A2.

K-feldspar

The partial mixing properties for orthoclase in the alkali feldspar solid solution are calculated from a binary sub-regular model taken from Perchuk et al. (1990) or:

$$G^e = X_K X_{Na}(W_{KNa}X_K + W_{NaK}X_{Na}) \quad (A7)$$

where

$$W_{KNa} = (6560 - 2.486T + 0.074P)(1 - Z) + (7832.0 - 2.657T + 0.074P)Z$$

and

$$W_{NaK} = (4612 - 2.504T + 0.101P)(1 - Z) + (7594.0 - 5.931T + 0.142P)Z$$.

Here, Z is the degree of feldspar ordering and $RT\ln f_{H_2O}^o$ is taken from data base of Holland and Powell (1990).

A2 Calculation of alkali activities for Fig. 9a, b

Figure 9a, b were calculated by means of solving a series of non-linear thermodynamic equations ($\Delta G = 0$) for each mineral assemblage using the thermodynamic parameters and Mg-content of the rocks given in the caption for Fig. 9. The standard partial molar thermodynamic properties and parameters of the equation

of state for K^+, Na^+ and H^+ were taken from the data base of Shock and Helgeson (1988). In order to calculate the partial molar Gibbs' free energy for these species at the temperature and pressure of interest, Eq. (31) from Shock et al. (1989, p. 2162) was applied. The water dielectric constant, which is included in this equation, was calculated using the Kirkwood equation (cf. Pitzer 1983). The calculated free energies for K^+, Na^+ and H^+ were combined with the free energies of the solid phases from the data base of Holland and Powell (1990) in order to obtain the ΔG for reaction r2 (see Table A1):

$$\text{Sillimanite} + 2K^+ + H_2O + 5\text{quartz} = 2\text{K-feldspar} + 2H^+ \qquad \text{(A8)}$$

$\Delta G^o_{(A8)}$ was approximated by the values for $\Delta H^o_{(A8)}, \Delta S^o_{(A8)}, \Delta V^o_{(A8)}$ given in Table A1. These values are valid for a temperature interval of 400–800 °C and pressures 4–8 kbar (fit with $r^2 = 0.997$). Subsequently, reaction A8 was combined with reaction r3 to obtain reaction r8 (see Table A1).

N^{Kfs}_{Or} isopleths were calculated for K-feldspar in equilibrium with an H_2O fluid containing K^+, Na^+, and H^+ by determining the equilibrated value for $\log(a_{K^+}/a_{H^+})^{fl}$ from reaction r1 (Table A1) for independently varying values of N^{Kfs}_{Or} and $\log(a_{Na^+}/a_{H^+})^{fl}$. The N^{Pl}_{An} isopleths were calculated for the assemblage K-feldspar + plagioclase + quartz in equilibrium with an H_2O fluid containing K^+, Na^+, and H^+ by determining the equilibrated values for N^{Kfs}_{Or} and $\log(a_{K^+}/a_{H^+})^{fl}$ from reaction r1 (Table A1) and then independently varying N^{Pl}_{An} and $\log(a_{Na^+}/a_{H^+})^{fl}$ via the exchange reaction albite (in K-feldspar) = albite (in plagioclase).

N^{Opx}_{Al} isopleths were calculated for the assemblage orthopyroxene + K-feldspar + quartz in equilibrium with an H_2O fluid containing K^+, Na^+, and H^+ by determining the equilibrated values for N^{Kfs}_{Or} and $\log(a_{K^+}/a_{H^+})^{fl}$ from reactions r1 and r8 (Table A1) and then independently varying N^{Opx}_{Al} and $\log(a_{Na^+}/a_{H^+})^{fl}$. The N^{Bt}_{Eas} isopleths were calculated for the assemblage biotite + K-feldspar + quartz in equilibrium with an H_2O fluid containing K^+, Na^+, and H^+ by determining the equilibrated values for N^{Kfs}_{Or} and $\log(a_{K^+}/a_{H^+})^{fl}$ from reactions r3, r9 and r4 (Table A1) and then independently varying N^{Bt}_{Eas} and $\log(a_{Na^+}/a_{H^+})^{fl}$. Along with calculations for the N^{Opx}_{Al} and the N^{Bt}_{Eas} isopleths in the divariant field, the equilibrated Mg numbers for orthopyroxene and biotite are computed from reactions r5, r6, and r7. The lower boundary of the divariant field orthopyroxene + biotite + K-feldspar + plagioclase + quartz + fluid in Fig. 9a, b is calculated by determining the equilibrated values for N^{Opx}_{Mg}, N^{Opx}_{Al}, N^{Bt}_{Mg}, N^{Bt}_{Eas}, and N^{Kfs}_{Or} from reactions r1–r9 (Tables A1 and A2) for varying values of $\log(a_{K^+}/a_{H^+})^{fl}$ and $\log(a_{Na^+}/a_{H^+})^{fl}$ respectively. N^{Bt}_{Mg} equals N^{rock}_{Mg} along this boundary. The upper boundary of the divariant field orthopyroxene + biotite + K-feldspar + plagioclase + quartz + fluid in Fig. 9a, b is calculated by determining the equilibrated values for N^{Opx}_{Mg}, N^{Opx}_{Al}, N^{Bt}_{Mg}, N^{Bt}_{Eas}, and N^{Kfs}_{Or} from reactions r1–r9 (Table A1) for varying values of $\log(a_{K^+}/a_{H^+})^{fl}$ and $\log(a_{Na^+}/a_{H^+})^{fl}$ respectively. Along this boundary $N^{Opx}_{Mg} = N^{Mg}_{rock}$ and the amount of biotite in the system is equal to zero.

References

Aranovich LYa (1991) Mineral equilibria in multicomponent solid solutions (in Russian). Nauka Press, Moscow

Aranovich LYa, Newton RC (1997) H_2O activity in concentrated KCl and KCl–NaCl solutions at high pressures and temperatures measured by the brucite–periclase equilibrium. Contrib Mineral Petrol 127: 261–271

Aranovich LYa, Newton RC (1998) Reversed determination of the reaction: phlogopite + quartz = enstatite + potassium feldspar + H_2O in the ranges 750–875 °C and 2–12 kbar at low H_2O activity with concentrated KCl solution. Am Mineral 83: 193–204

Aranovich LYa, Shmulovich KI, Fed'kin VV (1987) The H_2O and CO_2 regime in regional metamorphism. Int Geol Rev 29: 1379–1401

Berman RG (1988) Internally-consistent thermodynamic data for minerals in the system Na_2O–K_2O–CaO–MgO–FeO–Fe_2O_3–Al_2O_3–SiO_2–TiO_2–H_2O–CO_2. J Petrol 29: 445–522

Berman RG, Aranovich LYa (1996) Optimized standard state and solution properties of minerals I model calibration for olivine, orthopyroxene, cordierite, garnet, and ilmenite in the system FeO–MgO–CaO–Al_2O_3–TiO_2–SiO_2. Contrib Mineral Petrol 126: 1–24

Burton KW, O'Nions RK (1990) The timescale and mechanism of granulite formation at Kurunegala, Sri Lanka. Contrib Mineral Petrol 106: 66–89

Duan Z, Moller N, Weare JH (1995) Equation of state for the NaCl–H_2O–CO_2 system. prediction of phase equilibria and volumetric properties. Geochim Cosmochim Acta 59: 2869–2882

Ebadi A, Johannes W (1991) Beginning of melting and composition of first melt in the system Qz–Ab–Or–H_2O–CO_2. Contrib Mineral Petrol 106: 286–295

Elkins LT, Grove TL (1990) Ternary feldspar experiments and thermodynamic models. Am Mineral 75: 544–559

Fonarev VI, Konilov AN (1986) Experimental study of Fe–Mg distribution between biotite and orthopyroxene at P = 490 MPa. Contrib Mineral Petrol 93: 221–235

Franz L, Harlov DE (1998) High-grade K-feldspar veining in granulites from the Ivrea–Verbano Zone, northern Italy: fluid flow in the lower crust and implications for granulite facies genesis. J Geol 106: 455–472

Friend CRL (1981) Charnockite and granite formation and influx of CO_2 at Kabbaldurga. Nature 294: 550–551

Fuhrman ML, Linsdley DH (1988) Ternary feldspar modelling and thermometry. Am Mineral 73: 201–215

Gerya TV, Perchuk LL (1990a) GEOPATH: a new computer program for geothermobarometry and related calculations with the IBM PC computer. IMA, 15th General Meeting. Beijing. Abstracts. V.2. P.1010

Gerya TV, Perchuk LL (1990b) GEOPATH – a thermodynamic database for geothermobarometry and related calculations with the IBM PC computer. The University of Calgary Press, Program and Abstract, pp 59–61

Gerya TV, Perchuk LL (1992) GEOPATH – a thermodynamic database for geothermobarometry and related calculations with the IBM PC AT/XT Computer. 29th International Geological Congress, Kyoto, Abstract2, p 1026

Gerya TV, Perchuk LL (1994) A new thermodynamic database for thermometry. International Mineralogical Association, 16th General Meeting, Pisa, Italy, Abstracts, p 142

Hansen EC, Newton RC, Janardhan AS (1984) Fluid inclusions in rocks from amphibolite-facies gneiss to charnockite progression in southern Karnataka, India: direct evidence concerning the fluids of granulite metamorphism. J Met Geol 2: 249–264

Hansen EC, Newton RC, Janardhan AS, Prame WKBN, Kumar R (1987) Charnockite in the making in southern India and Sri Lanka. Contrib Mineral Petrol 96: 225–244

Hansen EC, Newton RC, Janardhan AS, Lindenberg S (1995) Differentiation of late Archean crust in the eastern Dharwar craton, Krishnagiri-Salem area, south India. J Geol 103: 629–651

Harlov DE, Hansen EC, Bigler C (1998) Petrologic evidence for K-feldspar metasomatism in granulite facies rocks. Chem Geol 151: 373–386

Harlov DE, Wirth R (2000) K-feldspar-quartz and K-feldspar–plagioclase phase boundary interactions in garnet–orthopyroxene gneiss's from the Val Strona di Omegna, Ivrea–Verbano Zone, northern Italy. Contrib Mineral Petrol (in press)

Hiroi Y, Asami M, Curray PG (1990) Arrested charnockite formation in Sri Lanka: field and petrographic evidence for low-pressure conditions. Proc NIPR (Symposium on Antarctic Geoscience) 4: 213–230

Hoernes S, Fiorentini E, Hoffbauer R (1991) Oxygen and carbon isotope ratios in high-grade rocks from Sri Lanka as a monitor of fluid–rock interaction. In: Kröner A (ed) The crystalline crust of Sri Lanka, part I. Summary of research of the German–Sri Lankan Consortium, Geol Surv Dept Sri Lanka Prof Pap 5: 225–236

Holland TJB, Powell R (1990) An enlarged and updated internally consistent data set with uncertainties and correlations: the system K_2O–Na_2O–CaO–MgO–MnO–FeO–Fe_2O_3–Al_2O_3–TiO_2–SiO_2–TiO_2–C–H_2–O_2. J Met Geol 8: 89–124

Hovis GL (1986) Behavior of alkali feldspars: crystallographic properties and characterization of composition and Al–Si distribution. Am Mineral 71: 869–890

Icenhower JP, London D (1997) Partitioning of fluorine and chlorine between biotite and granitic melt: experimental calibration at 200 MPa H_2O. Contrib Mineral Petrol 127: 17–29

Jackson DH, Mattey DP, Harris NBW (1988) Carbon stable isotope analysis of fluid inclusions by stepping heating. Mem Geol Soc India 11: 149–158

Janardhan AS, Newton RC, Smith JV (1982) Ancient crustal metamorphism at low P_{H2O}: charnockite formation at Kabbaldurga, south India. Nature 278: 511–514

Kehelpannala KVW, Ratnayake NP (1999) Evidence for post-metamorphic metasomatism of high-grade orthogneiss's from Sri Lanka. Gondwanna Res 2: 167–184

Korzhinskii DS (1959) Physical–chemical basis of the analysis of the paragenesis of minerals. Consultant Bureau Inc, New York

Korzhinskii DS (1962) The role of alkalinity in the formation of charnockitic gneiss's (in Russian). Trudy Vost-Sibir Inst Acad Nauk SSSR Ser Geol 5: 50–61

Kröner A, Cooray PG, Vintage PW (1991) Lithotectonic subdivision of the Precambrian basement in Sri Lanka. In: Kröner A (ed) The crystalline crust of Sri Lanka, part I. Summary of research of the German–Sri Lankan Consortium; Geol Surv Dept Sri Lanka Prof Pap 5: 141–159

Manning DAC (1981) The effect of fluorine on liquidus phase relationships in the system Qz–Ab–Or with excess water at 1 kb. Contrib Mineral Petrol 76: 206–215

Mathavan V, Prame WKBN, Cooray PG (1999) Geology of the high grade Proterozoic terrains of Sri Lanka and the assembly of Gondwana: an update on recent developments. Gondwanna Res 2: 237–250

Milisenda CC, Pohl JR, Hofmann AW (1991) Charnockite formation at Kurunegala Sri Lanka. In: Kröner A (ed) The crystalline crust of Sri Lanka, part I. Summary of research of the German–Sri Lankan Consortium; Geol Surv Dept Sri Lanka Prof Pap 5: 141–159

Newton RC (1986) Fluids of granulite facies metamorphism. Adv Physical Geochem 5: 36–59

Newton RC (1995) Simple-system mineral reactions and high-grade metamorphic fluids. Eur J Mineral 7: 861–881

Newton RC, Aranovich LYa, Hansen EC, Vandenheuvel BA (1998) Hypersaline fluids in Precambrian deep-crustal metamorphism. Precamb Res 91: 41–63

Perchuk LL, Gerya TV (1992) The fluid regime of metamorphism and the charnockite reaction in granulites: a review. Int Geol Rev 34: 1–58

Perchuk LL, Gerya TV (1993) Fluid control of charnockitisation. Chem Geol 108: 175–186

Perchuk LL, Podlesskii KK, Aranovich LYa (1990) Thermodynamics of some framework silicates and their equilibria: application to geothermobarometry. In: Perchuk LL (ed) Progress in metamorphic and magmatic petrology. Cambridge University Press, Cambridge, pp 131–166

Perchuk LL, Gerya TV, Korsman K (1994) A model for charnockitisation of gneissic complexes. Petrology 2: 451–479

Pitzer KS (1983) Dielectric constant of water at very high temperature and pressure. Proc Natl Acad Sci USA 80: 4575–4576

Raith M, Srikantappa C (1993) Arrested charnockite formation at Kottavattam, southern India. J Met Geol 11: 815–832

Raith M, Hoernes S, Klatt E, Stähle HJ (1989) Contrasting mechanisms of charnockite formation in the amphibolite to granulite grade transition zones of Southern India. In: Bridgwater D (ed) Fluid movements–element transport and the composition of the deep crust; NATO ASIC 281, Kluwer, Dordrecht, pp 29–38

Roedder E (1984) Fluid inclusions. Reviews in mineralogy, vol 12. Mineralogical Society of America, Washington, DC

Safonov OG (1998) The role of alkalis in the formation of coronitic textures in metamangerites and metaanorthosites from the Adirondack Complex, United States. Petrology 6: 583–602

Safonov OG, Valley JW, Perchuk LL (1995) Isotopic and compositional characteristics of coexisting minerals from metagabbro, the Highland Complex, Sri Lanka. Petrology 5: 478–486

Safonov OG, Perchuk LL, Gerya TV (1999) Reaction textures and mobility of alkalis and Ca^{2+} during formation of patchy charnockites at Kurunegala, Sri Lanka. In: Murthy NGK, Ram Mohan V (eds) Charnockite and granulite facies rocks Proceedings of the International Symposium on Charnockite and Granulite Facies Rocks, Spec Publ N4. Madras, India, pp 239–251

Sandiford M, Powell R, Martin SF, Perera LRK (1988) Thermal and basic evolution of garnet granulites from Sri Lanka. J Met Geol 6: 351–364

Santosh M, Harris NBW, Jackson DH, Mattey DP (1990) Dehydration and incipient charnockite formation: a phase equilibria and fluid inclusion study from south India. J Geol 98: 915–926

Santosh M, Yoshida M, Nanda-Kumar V (1991) Fluid characteristics across a gneiss-charnockite reaction front in Sri Lanka: implication for granulite formation in Gondwanian deep crust. J Mineral Petrol Econ Geol 86: 27–44

Schenk V, Raase P, Schumacher R (1991) Metamorphic zonation and PT history of the Highland Complex in Sri Lanka. In: Kröner A (ed) The crystalline crust of Sri Lanka, part I. Summary of research of the German–Sri Lankan Consortium. Geol Surv Dept Sri Lanka Prof Pap 5, pp 150–163

Shmulovich KI, Graham CM (1996) Melting of albite and dehydration of brucite in H_2O–NaCl fluids to 9 kbars and 700–900 °C: implication for partial melting and water activities during high pressure metamorphism. Contrib Mineral Petrol 124: 310–382

Shock EL, Helgeson HC (1988) Calculation of thermodynamic and transport properties of aqueous species at high pressures and temperatures: correlation algorithms for ionic species and equation of state predictions to 5 kb and 1000 °C. Geochim Cosmochim Acta 52: 2009–2036

Shock EL, Helgeson HC, Sverjensky DA (1989) Calculation of thermodynamic and transport properties of aqueous species at high pressures and temperatures: standard partial molal properties of inorganic neutral species. Geochim Cosmochim Acta 53: 2157–2183

Stähle H, Raith M, Hoernes S, Delphs A (1987) Element mobility during incipient granulite formation at Kabbaldurga, southern India. J Petrol 28: 803–834

Thompson JB Jr (1959) Local equilibrium in metasomatic processes. In: Abelson PH (ed) Research in geochemistry. Wiley, New York, pp 427–457

Touret JLR (1995a) Brines in granulites: the other fluid. Bol Soc Espan Mineral 18/1: 250–252

Touret JLR (1995b) The role and nature of fluids in the continental lower crust. In: Yoshida M, Santosh M (eds) India and Antarctica during the Precambrian, Mem 34, Geol Soc Bangalore, India, pp 143–160

Vielzeuf D, Clemens JD (1992) The fluid absent melting of phlogopite + quartz: experiments and models. Am Mineral 77: 1206–1222

Wirth R, Voll G (1987) Cellular intergrowth between quartz and sodium-rich plagioclase (myrmekite) – an analogue of discontinuous precipitation in metal alloys. J Mater Sci: 22: 1913–1918

Yoshida M, Santosh M (1994) A tectonic perspective of incipient charnockites in East Gondwanna. Precamb Res 66: 379–392

Yoshida M, Kehelpannala KVW, Hiroi Y, Vintanage PW (1990) Sequence of deformation and metamorphism of granulites of Sri Lanka. J Geosci, Osaka City Univ 33: 69–107